Universiteit Utrecht

IMAU
Institute for Marine and Atmospheric research Utrecht

Faculty of Science

Iceberg production on Antarctica

Bachelor Thesis

Adriaan Groot

TWIN

Supervisors:

Dr. R.S.W. van de Wal
Institute for Marine and Atmospheric Research Utrecht

Dr. B. de Boer
Institute for Marine and Atmospheric Research Utrecht

June 18, 2018

Abstract

Structural failure of ice cliffs could potentially contribute significantly to major ice retreat of the Antarctic ice sheet. In the future, this could result in an increase of global mean sea level rise. We discuss two parametrisations for ice wastage due to ice cliff failure calving. We apply the parametrisations by implementing a module to the existing 3D Antarctic model ANICE. An analytical comparison between calving parametrisations favours a parametrisation from Schlemm and Levermann (2018) over a parametrisation from Pollard et al. (2015). Simulations that apply a sudden increase in temperature show that cliff failure calving has no significant influence during cold climate situations, but can contribute up to 11% of global sea level rises during warm climate situations. Applying ice shelf removal mechanisms show that ice sheets are especially vulnerable to cliff failure calving when ice shelves retreat. Cliff failure calving causes retreated ice sheets to recover more slowly and could reduce return rates by up to 38%. RCP enforced simulations imply 0.16 metres of additional global sea level rise due to cliff failure calving by 2500.

Contents

1 Introduction

The ice sheet on Antarctica is one of the two large ice sheets that exist in our current climate. It is quite uncertain how the Antarctic ice sheet responds to climate change. Global warming could lead to an increase of the production of icebergs on Antarctica. Icebergs are produced on Antarctica due to multiple processes. One of these processes is the structural failure of ice cliffs due to a combination of causes. Due to crevasses in these ice cliffs, they collapse under their own weight. These cliffs then collapse into the ocean becoming icebergs, drift off and are finally disintegrated by oceanic melting. In recent years, ice cliff failure received a increased amount of attention due to a paper published by DeConto and Pollard (2016). In this article the authors investigate "the rise in global mean sea level of 6-9 metres during the last interglacial (130,000 to 115,000 years. ago)". An interglacial is part of a glacial cylce, which also includes a glacial period. The interglacial period is marked by warmer temperatures and glacier retreats and the glacial period is marked by colder temperatures and glacier advances (Severinghaus and Brook, 1999). The significant rise in sea level during the last interglacial corresponds with a not so significant rise in temperature during that same period of time. Furthermore, previous models could not explain such a rise in sea level (e.g Pollard et al. (2015)). DeConto and Pollard (2016) therefore concluded that there must be an additional process at work on Antarctica that caused this unexplained rise in sea level. They suggested the process of cliff failure combined with another process called hydrofracturing, which involves melting water and rain draining into ice crevasses on ice shelves. The mechanisms that drive these processes will be discussed in chapter 2.1.

By implementing these processes into their model, DeConto and Pollard (2016) found that " Antarctica has the potential to contribute more than a metre of sea-level rise by 2100 and more than 15 metres by 2500, if emissions continue unabated". Especially the estimate for 2500 clashes with previous ideas about the quantity of global mean sea level rise, which are generally much lower. For example, Church et al. (2013) predicts a sea level rise of less than 7 metres by 2500 under similar circumstances. The reason for this relatively high rise in sea level compared to previous results is the nature of cliff failure. At the moment, Antarctica has almost no free ice cliffs as they are all kept in place by ice shelves. These ice shelves provide a supporting force that prevents the ice cliffs from falling into the sea. Once these shelves melt due to increased temperatures, they will no longer support the ice cliffs, which gives way to the structural failure and disintegration of these cliffs. This could result in an increased rate of ice discharge on Antarctica which will consequently result in an increase of global sea level.

In this thesis, I will investigate whether cliff failure is indeed a big factor of the ice mass balance of the Antarctic ice sheet and whether it has a significant influence on its ice loss. Firstly, I will try to reproduce the results found by DeConto and Pollard (2016) by using the existing 3D Antarctica ice model ANICE developed by de Boer et al. (2013). This model was previously used to simulate past behaviour of Antarctic ice and will be further discussed in chapter 3.1. I will then discuss the validity of the parametrisation of ice cliff failure by Pollard and DeConto as described in Pollard et al. (2015) both analytically and based on model output. Furthermore, I will discuss an alternative parametrisation on cliff failure by Schlemm and Levermann (2018) based on a 2D Navier Stokes equation. Moreover, I will study what the influence of ice cliff failure is on the ice mass balance on Antarctica compared to other processes such as basal melt, surface melt and discharge of ice shelves. These experiments involve running the ANICE model using different scenarios involving rising or fluctuating temperatures as well as tests that have sudden removal of ice shelves. This will give an insight into how cliff failure might behave under different circumstances as well as give feedback on how well the parametrisation fits reality. Likewise, I will do tests that cover circumstances that correspond with the last glacial cycle to see how much ice cliff failure should be observed during different stages of a glacial cycle. This will provide an insight into what stages of the glacial cycle are most influenced by cliff failure. Finally, similarly to DeConto and Pollard (2016), I will simulate various future scenarios and reach a conclusion regarding the main research question of this thesis: What is the influence of 'ice cliff failure' on the degradation of ice on Antarctica and consequently the rise of global sea levels?.

2 Theory

2.1 Cliff failure and shelf calving

Ice on Antarctica falls into two categories. Firstly, there is continental ice, which is ice that is part of the massive grounded Antarctic ice sheet. The Antarctic ice sheet is usually subdivided into two ice sheets, the west Antarctic ice sheet (WAIS) and the east Antarctic ice sheet (EAIS) as can be seen in figure 1. Secondly, there is floating ice, which is ice that is part of ice shelves that float on the ocean surrounding Antarctica. These shelves include a few dozen minor ice shelves as well as two major shelves, the Ross ice shelf and the Filchner-Ronne ice shelf.

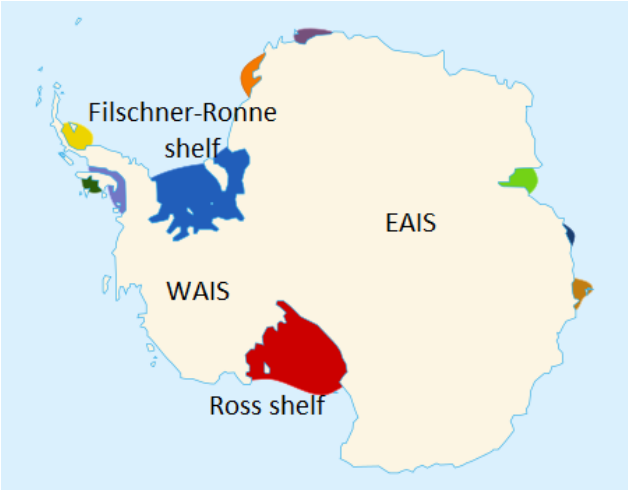

Figure 1: Schematic map of Antarctica. Courtesy of Dimitri Torterat (Edited). Ice shelves are given a colour.

The location where the ice sheet meets the ice shelf is called the grounding line. The grounding line (figure 2a) is the last place where ice is still in contact with the underlying bedrock. The boundary between grounded ice and floating ice is determined by the densities of ice and seawater. Namely, at the grounding line the ratio of ice height and seawater depth is given by $\rho_i/\rho w$, where $\rho_i = 910\text{kg/m}^3$ is the density of ice and $\rho_w = 1028\text{kg/m}^3$ is the density of seawater at circumstances comparable to those on Antarctica (de Boer et al., 2013).

The mass loss of ice shelves is influenced by multiple processes, which are depicted in figure 2. One of these processes is ice calving, which is the breaking off of ice under the influence of their own weight in combination with crevasses in the ice. These crevasses form due to shear stress from the weight of the ice sheet and shelf as well as a process called hydrofracturing. Hydrofracturing occurs when surface melt or rainwater drains into existing crevasses and deepens them by means of melting the surrounding ice. A parametrisation of ice shelf calving will follow in chapter 2.3.3.

When an ice shelf has disappeared completely due to melt and calving it reveals an ice cliff (figure 2f). Since there is no ice shelf supporting it any more, it is prone to cliff failure. This is shown in figure 3. Cliff failure occurs when the glaciostatic pressure from the weight of the grounded ice combined with the crevasses formed by stress and hydrofracturing outweigh the hydrostatic pressure from the ocean water. When this happens, a part of the cliff collapses and falls into the ocean. This may also be called calving and we shall therefore distinguish between shelf calving and cliff calving. Parametrisation of this process will be discussed in chapters 2.3.1-2.3.2. The exact mechanics of the calving process remain poorly understood however.

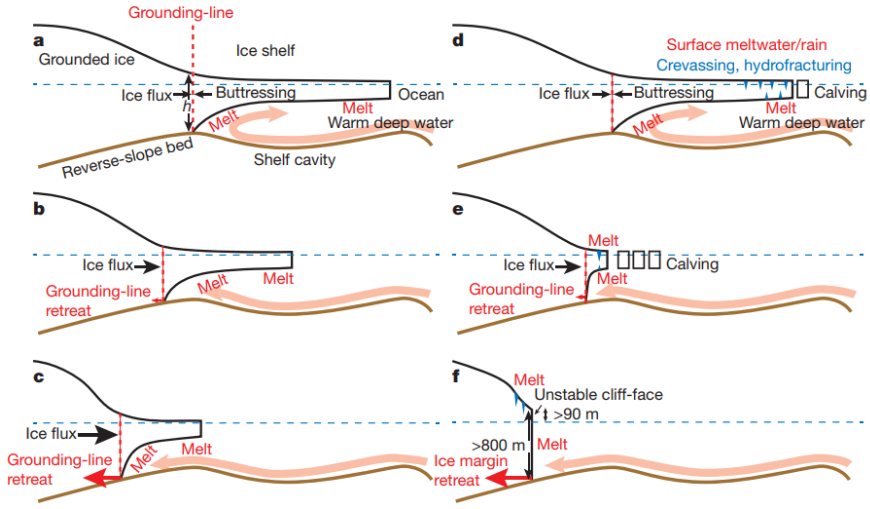

Figure 2: Schematic representation of processes that influence shelf melt and calving (DeConto and Pollard, 2016)(Edited). Ice is gained, mostly by flux from the inside of the Antarctic ice sheet, where it is accumulated by snowfall. figure 2a-f represent a situation where more ice on the shelves is lost than gained. Firstly, relatively warm ocean water melts ice at the bottom of shelves. (figure 2a). The grounding line is contained by buttressing. Buttressing is the process of supporting a structure by hanging onto it (e.g. stone structures on temples). In this case, the ice shelf supports the ice sheet by butressing onto it. This results in the ice shelf holding the ice sheet into place. When the shelf loses mass, the buttressing reduces and the grounding line retreats (figure 2b-c). The same happens when ice calving breaks of parts of the ice shelf (figure 2d-e). These processes may finally result in the reveal of a cliff face where grounded ice adjoins the ocean (figure 2f). When this happens, there is way for ice margin retreat due to ice cliff failure.

2.2 Critical height for cliff failure

When an ice cliff gets taller it becomes more unstable. We therefore use a critical height to determine at what point a cliff will fail structurally and collapse. We first discuss an expression for this critical height from Bassis and Walker (2011), which is one of the most complete expressions currently available. We then also discuss a critical value from Pollard et al. (2015) which sets a similar condition as a critical height. However, there is no precise knowledge available into the processes that determine when an ice cliff fails structurally. This means there is a need for semi-empirical evidence to get anything that can be used.

Bassis and Walker (2011) focus on crevasses in the ice, based on the assumption that "an iceberg will detach when either a surface crevasse or a bottom crevasse penetrates the entire ice thickness or some critical fraction thereof". Firstly, an expression for the horizontal (σ_{xx}) and vertical (σ_{zz}) stress tensors is derived, based on the assumption that "the width of the glacier is large so that horizontal deviatoric and shear stresses associated with the fjord walls can be neglected, over length scales that are large compared with the ice thickness"(Macayeal, 1989). (σ_{xx}) and (σ_{zz}) are given by:

$$\sigma_{zz} = \rho_i g z - S_{xx}, \tag{1}$$

$$\sigma_{xx} = \rho_i g z + S_{xx}, \tag{2}$$

where S_{xx} is the 'vertical deviatoric stress' in the x direction and onto the x direction, which is the horizontal direction in this case. So hereafter an expression for S_{xx} is derived by using the force balance (figure 3) "between the weight of the ice and the water-air in front of the ice". It then follows that "S_{xx} is determined by balancing the depth-averaged horizontal stress with the depth-averaged pressure due to water at the interface adjacent to the ice cliff(van der Veen, 1996)":

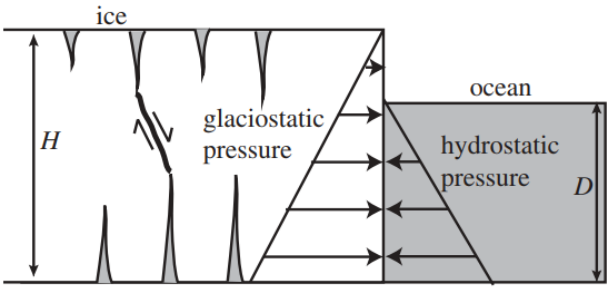

Figure 3: Schematic representation of the force balance between grounded ice and ocean water (Bassis et al., 2017). The weight of the grounded ice puts a glaciostatic pressure on the ocean, which in turn puts a hydrostatic pressure on the grounded ice. Crevasses form in the grounded ice due to shear stress and hydrofracturing

$$\int_0^H (S_{xx} - \rho_i g z)dz = \int_0^D -\rho_w g z dz. \tag{3}$$

.

Here H is the height of the ice from the seabed, D is the sea level height from the seabed and $g = 9.81\text{m/s}^2$ is the gravitational constant. Solving the integrals in equation (3) gives us an expression for S_{xx} in terms of H and D:

$$S_{xx} = \frac{1}{2}\rho_i g H \left(1 - \left(\frac{\rho_w}{\rho_i}\right)\left(\frac{D}{H}\right)^2\right). \tag{4}$$

Then the Nye-zero stress model is used to derive an expression for surface (d_s) and bottom (d_s) crevasses (Nye, 1957):

$$d_s = \frac{S_{xx}}{\rho_i g}, \tag{5}$$

$$d_b = \frac{\rho_i}{\rho_w - \rho_i}\left(\frac{S_{xx}}{\rho_i g} - H_s\right). \tag{6}$$

Here H_s is the height above buoyancy, which is the part of the height of the ice cliff that extends beyond the height that the ice cliff would have if it was at flotation, defined as follows:

$$H_s = H - \frac{\rho_w}{\rho_i} D. \tag{7}$$

Combining equations (4) and equations (5) and (6) we then get an expression for crevasse depths which are solely dependent on ice height (H) and water depth (D):

$$d_s = \frac{1}{2}\left(1 - \left(\frac{\rho_w}{\rho_i}\right)\left(\frac{D}{H}\right)^2\right) H, \tag{8}$$

$$d_b = \frac{\rho_i}{\rho_w - \rho_i}\left(\frac{\rho_w}{\rho_i}\frac{D}{H} - \frac{1}{2}\left(1 + \left(\frac{\rho_w}{\rho_i}\right)\left(\frac{D}{H}\right)^2\right)\right) H \tag{9}$$

.

Figure 4 shows the surface and bottom crevasses as function of the depth-height ratio. A maximum amount of penetration occurs at $D/H = 0$, where $d_s = 0.5H$ as well as at $D/H = 1$, where $d_b = 0.5H$. Furthermore,

there is not much variation in this parametrisation of the depth of crevasses as the minimum value of the combined crevasses occurs at $D/H \approx 0.65$, where $d_s + d_b = 0.26H$. Moreover, Bassis and Walker (2011) do not consider extra deepening of crevasses due to hydrofracturing.

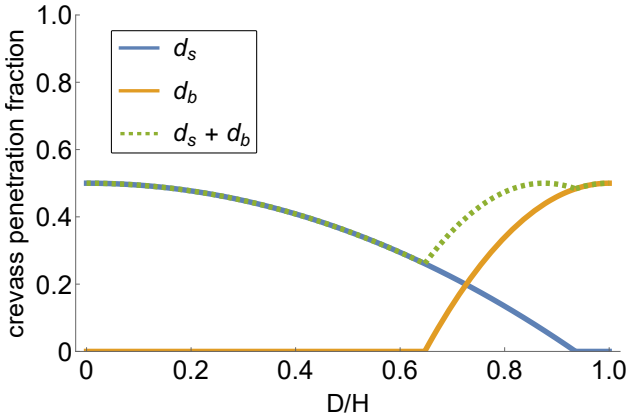

Figure 4: Fraction of the ice penetrated by crevasses as function of the ratio of water depth to ice thickness. The blue and orange line represents respectively the fraction of the ice that is penetrated by surface crevasses and the fraction that is penetrated by bottom crevasses. The green dashed line is the fraction of the ice that is penetrated by either surface or bottom crevasses. (A similar graph appears in (Bassis and Walker, 2011))

The complete penetration of an ice column would be sufficient for the ice column to break off. However, it is not necessary. Namely, "For an ice cliff to be stable, the depth-averaged shear stress must be less than the depth-averaged yield stress" (Bassis and Walker, 2011). Following this, the principal stresses are approximated as σ_{xx} and σ_{zz}. If the depth-averaged shear strength of ice is then τ_c and the total shear stress is then $\Delta\tau$, the requirement for an ice cliff to be stable is expressed as follows:

$$\Delta\tau = \frac{1}{2}\left(\sigma_{xx} - \sigma_{zz}\right) = S_{xx} \leq \tau_c. \tag{10}$$

By using equations (4) and (10), this then gives us a maximum height (H_c) for stable cliffs in terms of the depth-averaged shear strength of ice (τ_c) and the depth of the ocean (D):

$$H_c = \frac{\tau_c}{\rho_i g} + \sqrt{\left(\frac{\tau_c}{\rho_i g}\right)^2 + \frac{\rho_w}{\rho_i} D^2}. \tag{11}$$

There is some discontinuity between Bassis and Walker (2011) and Bassis et al. (2017) on how the depth-averaged shear strength of ice (τ_c) is defined. Furthermore, there are some linear factors added, for example $(1-r)\tau_c$ instead of τ_c to account for crevasse penetration r. However, at one point the value of τ_c has to be determined empirically. Therefore, linear adjustments do not have an influence on the final expression. This empirical analysis is done in Bassis et al. (2017) by using ice height and seawater depth of existing cliffs as can be seen in figure 5. A value that corresponds with $\tau_c = 400$kPa is chosen. However, there are too many observed cliffs that do not fit within this range and are thus stable despite being taller than the critical height depicted by the black line (figure 5). It is therefore a good idea to choose a more conservative value of $\tau_c = 600$kPa so that more cliffs fit within the boundaries. From now on, we shall set τ_c to be 600kPa when considering this particular expression for the critical height. We then get from equation (11) that a dry cliff, a cliff that ends on land, has a critical height of approximately 135 metres.

By filling in equation (11), we now have an expression that tells us whether a free standing ice cliffs is stable or not. In summary, given the water depth D, an ice cliff will be unstable when the following condition for the height H is met:

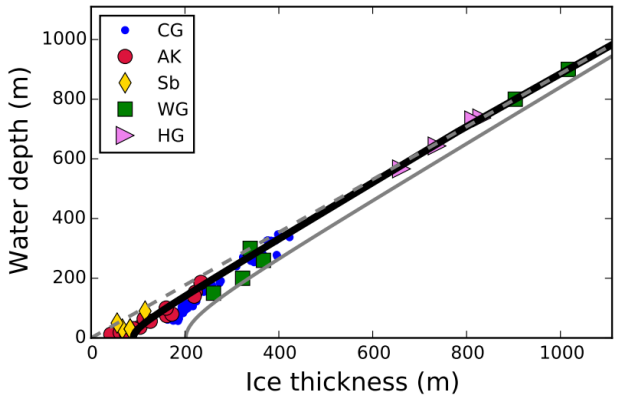

Figure 5: Fit of yield functions to observed ice thickness and water depth combinations (Bassis et al., 2017). The black and grey lines represents the critical height as function of the water depth for respectively $\tau_c = 400$kPa and $\tau_c = 800$kPa. Everything under these lines is considered unstable and will break off. The dashed line represents the bouncy limit for ice. Everything above this line floats and is not considered an ice cliff any more. The symbols represent existing cliffs that are observed at the Columbia Glacier (CG), Alaska (AK), Svalbard (Sb), West Greenland (WG) and the Helheim Glacier (HG).

$$H > \left(68 + \sqrt{4618 + 1.14D^2}\right) \text{m}. \tag{12}$$

A different condition is used by Pollard et al. (2015). Firstly, the ice yield strength is defined to be 1MPa, which is consistent with Bassis and Walker (2011). Then a force balance is derived similar to equation (10), but taking into account crevasses in the ice formed by stress on the surface (d_s) and on the bottom (d_b) as well as crevasses formed by hydrofracturing (d_w). Furthermore, the assumption that the ice cliff is at the grounding line is used. Equation (10), for stable cliffs then becomes (Pollard et al., 2015):

$$\frac{\tau_c}{\rho_i g}\left(H - (d_s + d_b + d_w)\right) < H\left(1 - \frac{\rho_i}{\rho_w}\right)(d_s + d_b)\,. \tag{13}$$

The derivation for this inequality will not be given in this thesis, because it is not given by Pollard et al. (2015) and it is not straightforward. The expressions for the depth of crevasses due to stress (d_s and d_s) are the same as those used by Bassis et al. (2017) (equations (8) and (9)). The crevasse depth due to hydrofracturing (d_w) is given by (DeConto and Pollard (2016)):

$$d_w = \begin{cases} 0 & \text{for } R \leq 1.5\text{m yr}^{-1} \\ 600(R - 1.5) & \text{for } 1.5\text{m yr}^{-1} < R \leq 3\text{m yr}^{-1} \\ 100R^2 & \text{for } R > 3\text{m yr}^{-1}. \end{cases} \tag{14}$$

Here R is the annual surface melt and rainfall available after refreezing in m yr^{-1}. This relation is adopted from Nick et al. (2012), who used coefficients in the range of 20-30 and had a linear relation. Figure 6 shows the crevasse depth due to hydrofracturing as function of R. This parametrisation results in there being at least 1.5 metres of liquid water needed to start hydrofracturing. Moreover, after this amount is reached, every metre of water results in a deepening of crevasses of hundreds of meters.

Using the value of $\tau_c = 1$MPa, Pollard et al. (2015) then defines a critical ice height above water line $h_{cr} = \tau_c/\rho_i g \approx 113$m. This does not represend an actual critical height above water however, but rather just a critical value that can be used to enforce a condition on the ice cliff. Furthermore, using the grounding line condition we find that for this case the glacier freeboard, which is the height of the part of the ice that extends above the water, is as follows:

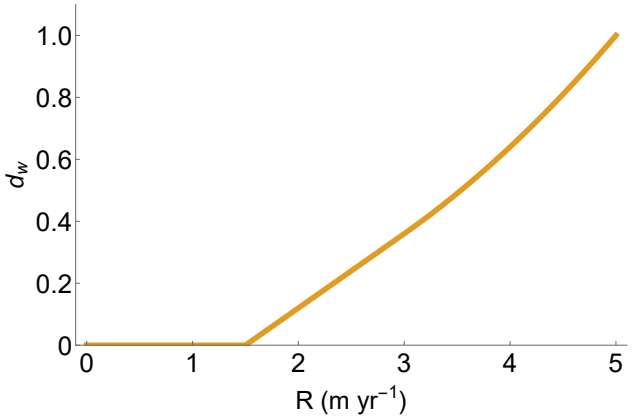

Figure 6: Crevasse penetration ratio due to hydrofracturing as a function of the available liquid water. A typical ice height of 2500 metres is used.

$$H_s = H(1 - \rho_i/\rho_w). \tag{15}$$

We now have another, different condition that tells us whether an ice cliff is stable or not. Namely, given the crevasse depths d_s, d_b and d_w and the cliff height, a cliff will be unstable if the following condition is met:

$$h_{cr} < H_s \left(\frac{d_s + d_b}{H - (d_s + d_b + d_w)} \right), \tag{16}$$

where $h_{cr} \approx 113$m and H_s, d_s, d_b and d_w are given by respectively equations (15), (8), (9) and (14). The assumption is made that d_s, d_b and d_w are defined in such a way that $d_s + d_b + d_w \leq H$.

2.3 Ice wastage

In section 2.2 a critical height for cliff failure is discussed. We will now discuss two parametrisations that deal with how much ice is removed from the grounded ice sheets when a cliff fails structurally. In other words, how much 'wastage' of ice there is. On top of this, a parametrisation for the removal of ice from ice shelves due to calving will be discussed.

2.3.1 Parametrisation of cliff failure using Pollard et al.

One option for parametrisation of ice cliff wastage is discussed in Pollard et al. (2015) and follows directly from the condition in equation (16). A maximum horizontal ice wastage of 3km yr^{-1} is chosen based on "observations of ice vs. terminus velocities at Jakobshavn Isbrae (Joughin et al. (2014); ∼12km yr^{-1}) and Crane Glaciers terminus retreat (Scambos et al. (2011); ∼5km yr^{-1})". This wastage is horizontal, which means that the ice column will in theory break off in the entirety of its height for a distance that is given by the wastage. The maximal value of 3km yr^{-1} is chosen conservatively with these observations in mind. However, some questions can be raised about the correctness of this value. Some critiques regarding this subject shall be discussed in chapter 4. This maximum value is then implemented with the idea that when the condition in equation (16) is met and has a substantial margin, there is maximum cliff calving and when the condition is not met, there is no cliff calving at all. This results in the following expression for the horizontal wastage term for cliff calving W in m yr^{-1} (Pollard et al., 2015):

$$W = 3000 \max\left[0, \min\left[1, \frac{1}{20}\left(H_s\left(\frac{d_s + d_b}{h - (d_s + d_b + d_w)}\right) - h_{cr}\right)\right]\right]. \tag{17}$$

As intended, this wastage term acts like a ramp, where you usually either break off a full 3km yr^{-1} of ice or no ice at all. This can be seen in figure 7, where the wastage term is shown as a function of ice height above sea level for certain given crevasse depths. A more in depth analysis will follow in chapter 4.

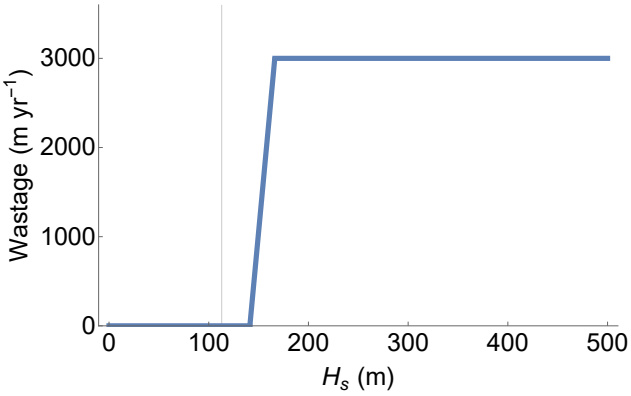

Figure 7: Horizontal wastage for cliff calving in m yr^{-1} as function of the glacier freeboard in m. The blue line represents the wastage term (W) in equation (17). Values of crevasses that are used for this example are $d_s + d_b = 0.4H$ and $d_w = 0.1H$, which means the crevasses reach through half the height of this cliff. The thin grey line represents the critical value $h_{cr} \approx 113m$.

2.3.2 Parametrisation of cliff failure using Schlemm and Levermann

Another parametrisation of cliff failure wastage comes from Schlemm and Levermann (2018). This parametrisation also assumes a maximum shear stress of ice of 1MPa. It then uses a 2D stokes equation and the conservative assumption that the calving rate has a characteristic response time of 1 year to derive the following expression for the horizontal ice wastage:

$$W_2 = a \cdot \exp\left(\frac{w}{w_s}\right)\left(\exp\left(\frac{H_s - F_c}{F_s}\right) - 1\right). \tag{18}$$

Here w is the ratio between the sealevel and the ice cliff height and H_s is the glacier freeboard. Schlemm and Levermann (2018) do not assume flotation, so $w = D/H$ and $H_s = H - D$. Furthermore, Schlemm and Levermann (2018) set the scaling parameters to $w_s = 0.45$, $F_s = 2455$m, $W_0 = 3318$m and the critical freeboard $F_c = 144$m based on the solution of the 2D stokes equation. We then get the expression for the horizontal wastage W_2 in m yr^{-1} in terms of the cliff height H and the water depth D:

$$W_2 = 3318 \cdot \exp\left(\frac{D}{0.45H}\right)\left(\exp\left(\frac{H - D - 144}{2455}\right) - 1\right). \tag{19}$$

Figure 8 shows the horizontal ice wastage W_2 in equation (19) as a function of ice height and water depth. Counter intuitively however, for small water depths, the wastage gets smaller with lower water depths. This seems like an error, since the water holds the ice cliff into place. A further analysis and comparison with the first wastage term will follow in chapter 4.

2.3.3 Parametrisation of shelf calving

Calving of shelves as described in chapter 2.1 is often done by simply removing parts of shelves that are lower than a certain height, where this height is a constant (e.g. de Boer et al. (2013)). A different approach is used by Pollard et al. (2015) similarly to the derivation of the expression for the wastage in equation (17). Firstly, an expression for crevasse depth due to extensional stress is derived for both bottom and surface

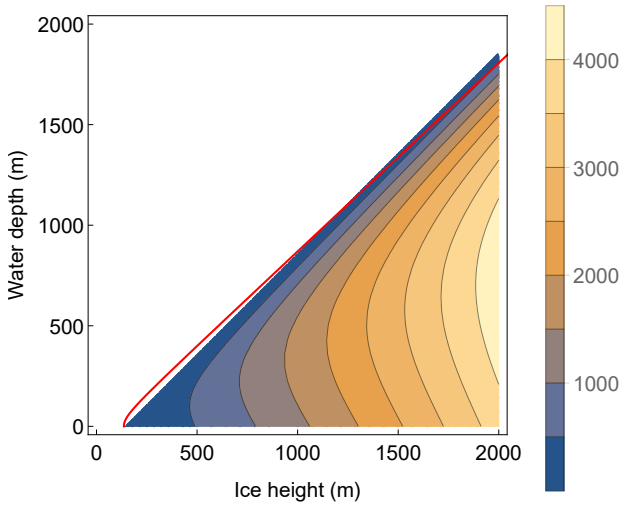

Figure 8: Contour plot of the horizontal wastage for cliff calving in m yr^{-1} as a function of ice height and water depth. Values of the wastage range between 0 and up to 4500 m yr^{-1} for the given heights and depths as depicted in the bar on the right. The white area represents cliffs that do not meet the required height of 144m. The critical height from Bassis et al. (2017) is depicted with a red line.

crevasses. These expressions are different from the ones for cliff failure calving (equations (8) and (9)) and are given by:

$$d_s = \frac{2}{\rho_i g}\left(\frac{\dot{\varepsilon}}{A}\right)^{\frac{1}{3}}, \tag{20}$$

$$d_b = \left(\frac{\rho_i}{\rho_w - \rho_i}\right)\frac{2}{\rho_i g}\left(\frac{\dot{\varepsilon}}{A}\right)^{\frac{1}{3}}, \tag{21}$$

where A is the vertical mean flow rate factor (as in de Boer (2012)), and $\dot{\varepsilon}$ is ice divergence. Calving can occur at any point in the shelf, so this includes the inner part, in contrary to cliff failure calving which only occurs at free standing cliffs at the boundary of ice sheets. Ice divergence is different at the boundaries of ice shelves from ice divergence at interior points. Pollard et al. (2015) use the following expressions:

$$\dot{\varepsilon} = \left(\frac{\partial u}{\partial x} + \frac{\partial v}{\partial y}\right), \tag{22}$$

$$\dot{\varepsilon} = A\left(\frac{\rho_i g h}{4}\right)^3, \tag{23}$$

where the partial derivatives in equation (22) is ice divergence in the horizontal directions. h is an adjusted average of heights of surrounding ice and will be discussed in chapter 3.2 as it depends on model specifications. Chapter 3.2 will also cover when to apply which of the two expressions as it depends on model specifications as well. When applying equation (23) to equations (20) and (21), they reduce to respectively $0.5h$ and approximately $3.8h$. This means when equation (23) is used, the ice is completely penetrated by crevasses, as $3.8h + 0.5hh$ is greater than h.

The expression for crevasses due to hydrofracturing is the same as for cliff failure and is therefore given by equation (14). Besides crevasses due to stress and hydrofracturing, Pollard et al. (2015) add another two expressions that contribute to the crevasse depth. One additional crevasse deepening term (d_a) is added to

account for the excessive calving at the edges of the Ross and FilchnerRonne ice shelves, where there is a relatively high ice speed:

$$d_a = \frac{h}{\ln(1.2)} \max\left[0, \ln\left(\frac{u}{1600}\right)\right]. \tag{24}$$

Here u is local ice speed and h is the same average of heights as in equation (23) when applied to the edge of the ice shelf and just the ice height H when applied to the interior of the shelf. As can be seen in figure 9, the d_a term only contributes when the local ice speed is higher than 1600m yr^{-1}, which is relatively high at ice shelf edges. From there it adds crevasse depth until the ice reaches a speed of 1920m yr^{-1}, from where the crevasse depth is equal to h.

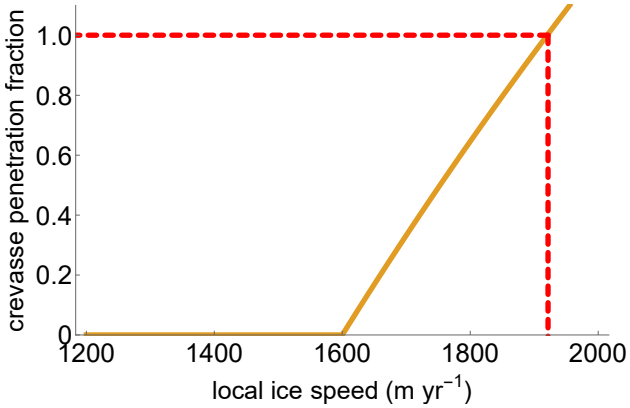

Figure 9: Crevasse penetration ratio due to high ice speeds as function of local ice speed. Penetration fraction is the fraction of h that is penetrated by crevasses.

Finally, a term that deals with unrealisticly small ice shelves is added:

$$d_t = h \max\left[0, \min\left[1, \frac{150 - h}{50}\right]\right]. \tag{25}$$

This has the effect of completely crevassing shelves under 100 metres as well as partly crevassing shelves between 100 and 150 metres. Pollard et al. (2015) set a requirement of 75% of the ice shelf to be penetrated by these crevasse terms and consequently define a horizontal wastage term, much like with cliff failure calving, for shelf calving to be:

$$C = 3000 \max\left[0, \min\left[1, 4\left(\frac{d_s + d_b + d_w + d_a + d_t}{h} - 0.75\right)\right]\right]. \tag{26}$$

As can be seen in figure 10, this term is just a linear progression in ice from 0m yr^{-1} at 75% crevasse penetration and 3000m yr^{-1} at complete penetration.

2.4 RCP

The Intergovernmental Panel on Climate Change (IPCC) uses so called Representative Concentrations Pathway (RCP) scenarios that represent possible future global CO_2 emission rates. The IPCC used four different pathways, RCP2.6, RCP4.5, RCP6.0 and RCP8.5, where the numbers represent global energy imbalances in W/m^2. These scenarios also come with a prediction on future temperatures as can be seen in figure 11. These predictions will be used in this thesis to predict future sea levels with calving processes in mind.

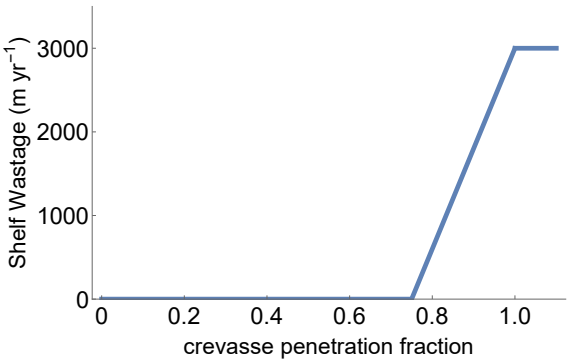

Figure 10: Horizontal shelf wastage as function of penetration fraction. Penetration fraction is the ratio of h that is penetrated by crevasses.

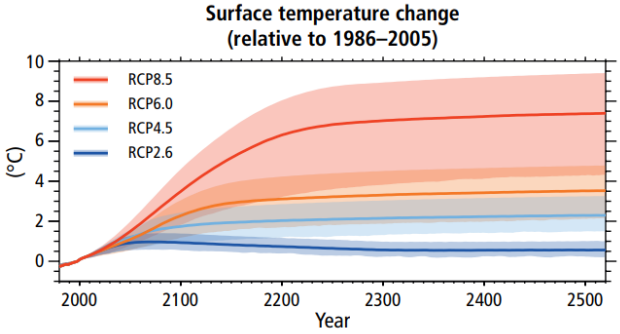

Figure 11: Projected global mean surface temperature change as simulated by Earth System Models (Pachauri et al., 2014).

3 Methodology

3.1 ANICE model

To study cliff failure calving the 3D Antarctica model ANICE by de Boer et al. (2013) is used. This model deals with many processes that influence Antarctica as well as other ice sheets, but only the pieces that are relevant to this thesis will be discussed. ANICE is an inverse forward model that is used to simulate Antarctica in the past by using benthic δ^{18}O data, a measure of the ratio of oxygen isotopes, as proxy for temperature which is used as constraint for the model. However, the model can also be used for future simulations. The model is written in Fortran. The models initial ice heights, temperature conditions, sea level etc. can be chosen freely. These conditions are chosen appropriately for different experiments as will be discussed in chapter 5.

ANICE consists of a raster of grid points that contain information about the particular place the grid points represent on Antarctica. The grid points are divided into five categories: ice sheet, grounding line, ice shelf, calving line and ocean as can be seen in figure 12. A grid point is assigned the type grounding line when it is part of an ice sheet and is adjacent to a grid point that is either ocean or ice shelf, representing the actual grounding line. A grid point assigned calving line is a part of an ice shelf and is adjacent to a grid point that is ocean. For this thesis grid points of 40 by 40 kilometres are used. As computational time rises quadratically by decreasing grid size, this is the middle ground between accuracy and computationally cheap model runs. To cover Antarctica and its surrounding ocean 141 by 141 grid points are used. The model is 3D in the sense that each grid point contains a variable for the ice height. Besides ice height, each grid point contains information on the height of the bedrock under the ice. The bedrock height changes dynamically depending on ice height, as the weight of the ice pushes it down.

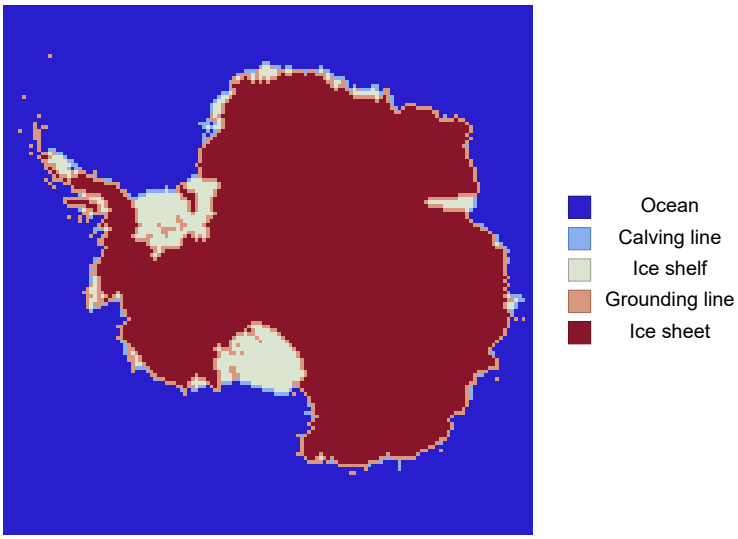

Figure 12: An example of grid point type distribution on Antarctica. This is the layout as represented by grid point types of present day Antarctica, thus the same conditions as in figure 1 in chapter 2.1.

ANICE calculates the contribution and removal of ice by processes such as melting, ablation, accumulation and refreezing by using parametrisations as found in de Boer et al. (2013). Melting happens at the surface but also below the ice shelves by means of warming by oceanic warmth. The yearly contribution and removal of ice by these processes are calculated and added up to form a mass balance per grid point. This mass balance is in the form of a volume, that is converted to a vertical ice height on the grid point. The ice also slides and flows from grid points to other grid points. The ice fluxes that are the result of this are also calculated by de Boer et al. (2013) by using centered difference discretisation. A grid point is surrounded by

four other grid points, which results in four outgoing fluxes per grid point. The ice lost through these fluxes is added to the grid points in their corresponding direction. Given the ice height on a grid point in a certain year, the ice height in a subsequent year is then calculated by applying the mass balance and in coming and out coming ice fluxes. The mass balance is applied first. This means that if the mass balance is negative and exceeds the available ice it is set to 100% of the available ice and the outgoing ice fluxes is set to zero. If the mass balance does not exceed the available ice, but the outgoing fluxes do, the fluxes are scaled over the four outgoing directions.

3.2 Application of the calving module

A module that calculates the quantity of cliff failure calving and shelf calving per grid point according to chapter 2 is added to the ANICE model. The output of this module is a vertical calving term that is applied to the mass balance which is then applied to the model as discussed in chapter 3.1.

3.2.1 Cliff failure calving

To determine how much cliff failure calving takes place on a grid point in a given year it is first checked whether the grid point in question is of the type grounding line and whether it is adjacent to any grid points of the ocean type. If either of these conditions are not met, calving is set to zero.

If both of these are satisfied and we are calculating cliff failure as in Schlemm and Levermann (2018), the height of the grid point (H) is checked against the critical height in equation (11). If it is lower than this height, calving is set to zero. If it is higher, the horizontal wastage is calculated based on ice height and water depth as in equation (19). Water depth at the grounding line (D) is calculated by subtracting sea level by bedrock height. This horizontal wastage is then multiplied by the amount of ocean type grid points that neighbour the grid point, because cliff failure happens on each of the grounding lines between these grid points. The resulting horizontal wastage is then applied as a vertical ice height reduction in the mass balance in the same way as in Pollard et al. (2015). The wastage is not applied horizontally, because that would mean having to store information on which part of the grid point is partially covered with ice and which is not. The implications of this numerical limitation are discussed in chapter 6.

If the a grid point is indeed part of the grounding line and borders ocean and we are calculating cliff failure calving as described in Pollard et al. (2015), the surface and bottom ice crevasses due to stress (d_s and d_b) are calculated using equations (5) and (6) respectively. The extra surface crevassing due to hydrofracturing (d_w) is then calculated using equation (14). The horizontal ice wastage per year (W) is then calculated using equation (17). This wastage term might still be zero, since the expression in equation (17) automatically imposed the condition in equation (16). The resulting horizontal wastage is then multiplied by the amount of surrounding ocean grid points and applied as a vertical ice height reduction in the mass balance in the same way as with cliff failure from Schlemm and Levermann (2018).

3.2.2 Shelf calving

To study the influence of cliff failure calving, we also need a way to implement shelf calving as it could remove shelves and expose cliffs which are then prone to cliff calving. We use the expressions by Pollard et al. (2015) from chapter 2.3.3 for this.

To determine how much shelf calving takes place on a grid point in a given year it is first checked whether a point is of the type calving line, which is per definition part of the ice shelf and next to the ocean. If this is the case, the adjusted height (h) that was introduced in chapter 2.3.3 from Pollard et al. (2015) is calculated. This adjusted height is used as well in Albrecht et al. (2011) and Pollard and DeConto (2012) as a way to calculate the actual grid ice thickness based on surrounding grid points to account for limitations due to relatively big grid size. The adjusted height is calculated as an average of the surrounding shelf grid points that are part of the shelf as well, which are all multiplied by a down stream thinning factor of:

$$L = 1 - w\left(1 - \exp\left(-\frac{\Delta x}{100}\right)\right). \tag{27}$$

Here Δx is the grid size in kilometres, which is 40km in our case and w is a weight given by:

$$w = \min\left[1, \frac{H}{h_a \exp\left(-\frac{\Delta x}{100}\right)}\right]. \tag{28}$$

Here H is the ice height of the grid point and h_a is the ice height of the adjacent point that has been checked to be a shelf grid point. This results in the expression for the adjusted height:

$$h = \sum_a \left(1 - \min\left[1, \frac{H}{h_a \exp\left(-\frac{\Delta x}{100}\right)}\right]\left(1 - \exp\left(-\frac{\Delta x}{100}\right)\right)\right) h_a. \tag{29}$$

Here a sums over the adjacent ice shelf grid points. This parametrisation is designed for sub-grid parametrisation, but is used for complete grid points here. The implications of this are discussed in chapter 6. As in Albrecht et al. (2011) and Pollard et al. (2015), when $H < h$, the expression in equation (23) is used to calculate ice divergence ($\dot{\varepsilon}$), which results in a completely crevassed grid point as discussed in chapter 2.3.3. Otherwise, the divergence of the ice is calculated as in equation (22) using a numerical approximation to calculate the ice divergence in both horizontal directions. A maximum of zero is imposed on the divergence for numerical convenience, since otherwise this would result in crevasses with negative depth. The ice divergence is then used to calculate surface and bottom crevasse depth due to stress (d_s and d_b) using equations (20) and (21).

Moreover, the crevasse depth due to hydrofracturing (d_w) is calculated using the expression in equation (14) using the available liquid water (R) which is calculated by adding rain- and melt water and subtracting refreezing of water on the grid point. Furthermore, the crevasse contribution that accounts for high local speeds in equation (24) is calculated using local ice speed (u) from the model. Then, the crevasse contribution due to unrealistically small shelves (d_a) is calculated using equation (25), which uses the adjusted height from equation (29).

Then finally, the horizontal shelf calving wastage per year (C) is calculated using the expression in equation (26) which uses all the crevasse depths calculated before. Similarly to cliff failure calving, this is then multiplied by the amount of surrounding ocean grid points and converted to a vertical ice height wastage and is used in the mass balance term of the model. Also, any ice under 100 metres is discarded to prevent unrealistically small shelf grid points to form adjacent to the grounding line, preventing ice cliff failure. This is consistent with the expression for d_t in equation (25), which is designed to remove small sub-grid shelf grid points, but does not work well enough on bigger grid points because it is applied as a horizontal wastage and can therefore never completely discard all the ice on a large grid point. Nevertheless, the expression for d_t is kept, since it still removes ice from shelves with heights between 100 and 150 metres. The initial ANICE settings use a height of 200 metres for this purpose, but results are similar.

3.3 Output of the model

The output of the model that is relevant to this thesis consists of grid point type fields such as the one in figure 12, ice height fields, surface height fields, cliff failure calving fields and shelf failure calving fields as well as data on total ice volume, ice volume on land, ice volume on shelves, total mass balance per year, total surface mass balance per year, total bottom mass balance per year, total cliff failure calving per year and total shelf calving per year. The fields give an idea as to where on Antarctica calving takes place and whether the ice sheets and shelves grow or shrink and in which direction. The cliff and shelf calving data is generated in such a way that other processes take priority such that when there is no ice available to be calved, no ice is reported to be calved away. This way, it is easier to compare simulations that do use calving

and ones that do not. Total ice volume on land is directly related to sea level and global sea level rise (S) can be computed using the following relation (de Boer et al., 2015):

$$S = \left(\sum_{i,j} H_{0af} - H_{af} + \min(0, H_b) - \min(0, H_{b0}) \right) \frac{40000 \times 40000}{O_{area}}, \tag{30}$$

where H_{0af} and H_{af} are ice thickness above flotation for the initial and final ice sheet in metres water equivalent. So H_{af} corresponds to one time step after H_{0af} and both are given by:

$$H_{af} = \frac{\rho_i}{\rho_w} H + H_b. \tag{31}$$

H is ice thickness in metres, H_b is bedrock topography in negative metres below sea level and $O_{area} = 3.62 \times 10^{14}$ m^2 is the area of the world's ocean, which is assumed to remain constant (de Boer et al., 2015).

4 A comparison of the calving parametrisations

This chapter contains a discussion on which cliff calving parametrisation is more accurate as well as which parametrisation is more suitable for practical use. This is a comparison between the parametrisation by Pollard et al. (2015) in equation (17) and the parametrisation by Schlemm and Levermann (2018) in equation (19).

Firstly, the parametrisation by Pollard et al. (2015) is entirely based on the premise that the ice cliff in question is at flotation at the grounding line. Namely, this is exactly what the cliff failure condition in equation (16) assumes, since it is based on a force balance for an ice cliff at floatation. However, it is completely possible for free standing ice cliffs to not be at flotation. Especially in warmer climates, where shelf bottom melt and calving is relatively large, which results in more free standing cliffs. This assumption is not made by Schlemm and Levermann (2018), who actually include the ratio between cliff height and water depth into the parametrisation.

Secondly, the maximum of 3000 metres per year of horizontal ice wastage that Pollard et al. (2015) use is completely arbitrary. Namely, it is 'conservatively' chosen on basis of two glaciers that have calving of 5 km yr^{-1} and 12 km yr^{-1}. In addition to this, it is based on calving rates of Arctic glaciers, which are not nearly as wide as some of the ice sheets on Antarctica and might therefore behave quite differently. Since the wastage term is designed in such a way that usually either no ice is calved or 3000 metres of ice is calved, this value that is set at 3000 metres is actually excessively influential in how much ice is calved. Were you to set this value to 5000 metres, you could expect about 5/3rds of the amount of calving that you saw before. You could argue that changing to a maximum of 5000 metres per year would remove ice quicker from a grid point where calving takes place, which would result in a lower ice height on that particular grid point and therefore this grid point would have a lower chance of calving again in the calving cycle that happens the year after that. This might mean that a steady state is met either way and that you have some lenience in how you choose your maximum calving parameter. To find out if this is the case we run the model under moderately warm and warm climate conditions, because this is when shelves disappear and therefore most calving takes place. The result of this experiment can be seen in figure 13. We compare between 3000 and 5000 metres per year and conclude that the result is significant. Namely, during the warm climate simulation, the difference between a maximum of 3000 and 5000 metres per year is approximately 1.5 metres of sea level rise, which is not quite 2/3rds more, but is still an increase in sea level rise of approximately 12%. We conclude that the value of 3000 is rather arbitrary and is not balanced by external influences when raised to a higher value.

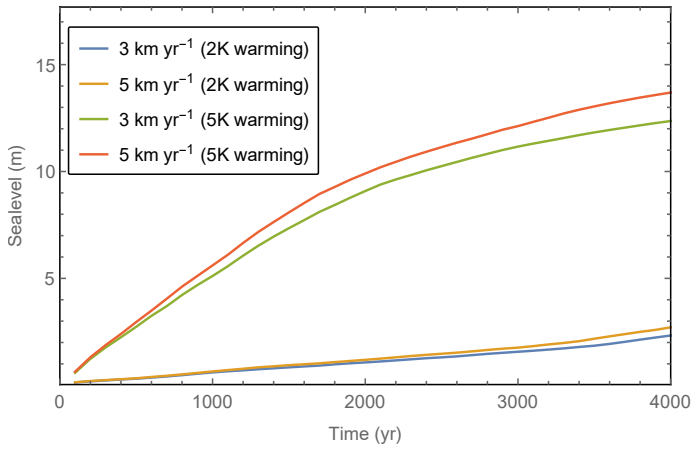

Figure 13: Sea level rise in moderately warm and warm climate simulations for different values of the maximum horizontal wastage per year. The blue and yellow line are sea level rises due to similar circumstances in a climate that is 2K warmer than present by using values for the maximum horizontal cliff failure calving of respectively 3 and 5 km yr^{-1}. Note, that the maximum values for the shelf calving have not changed, but a similar effect can be seen comparing those. The same applies for the green and red line, but 5K warming is applied instead.

Thirdly, one could argue whether using a drastic ramp (figure 7) as an expression for cliff calving is an accurate way of representing this process. Cliff calving is in principle a discrete process. A piece of ice breaks off, taking seconds to fall into the ocean. Which means a certain amount of ice is lost in a very short period of time. However, a single calving event usually only breaks off a fraction of the thousands of metres that is broken off in a year according to the horizontal term in equation (17) from Pollard et al. (2015) (Ryan et al., 2015). Also, this term covers the whole of a 40 kilometres long grid point. A calving event also only covers a fraction of these 40 kilometres. This means the wastage term from Pollard et al. (2015) (equation (17)) is the sum of a lot of single calving events. Logically, it makes more sense for it to be represented by a continuous function rather than a sudden ramp. Namely, this would ensure that grid points that would normally have no cliff calving at all, but are very close to having the required height, would have at least a little calving. This relates to the real life situation, since ice sheets are not made up of uniform squares of 40 by 40 kilometres, but have varying heights between different areas inside these squares. If you use the wastage term from Pollard et al. (2015) (equation (17)) however, you end up having no calving on squares that are only a few tens of metres lower than other cliffs where you end up with maximal calving. Again, this is where the calving parametrisation from Schlemm and Levermann (2018) (equation (19)) does a good job. As can be seen in figure 8, this parametrisation is rather smooth as it gets gradually higher with a higher ice height. On top of this, the expression from Schlemm and Levermann (2018) (equation (19)) is not very arbitrarily like the one from Pollard et al. (2015) (equation (17)), but is based of a 2D stokes analysis. Thus, you could argue that it has more of a connection to reality. An analysis that shows that the expression from Pollard et al. (2015) (equation (17)) is indeed a ramp for all circumstances can be found in appendix A. Nevertheless, figure 8 also shows that the expression from Schlemm and Levermann (2018) gets smaller with lower water depths for small water depths (the bottom area of figure 8). The only explanation for this can be an error in the expression from Schlemm and Levermann (2018).

Finally, the expression in equation (19) from Schlemm and Levermann (2018) corresponds fairly well with the critical height that was derived by Bassis et al. (2017) in equation (11), as can be seen in figure 14. It does not align perfectly, but this can be seen as an opportunity to improve on the expression from Schlemm and Levermann (2018) by imposing the requirement in equation (11) on the ice cliffs first. Thus, this is exactly what we do when using the expression from Schlemm and Levermann (2018) as was discussed in chapter 3.2. Besides, the condition from Schlemm and Levermann (2018) is usually more strict (but not always). As discussed in chapter 2.2, the critical height in equation (11) is based on empirical data from excising ice cliffs around the world (despite none of these cliffs actually being on Antarctica). It is therefore not unreasonable to conclude that at least the boundary condition of this the wastage term from Schlemm and Levermann (2018) (equation (19)) is fairly well adjusted to reality.

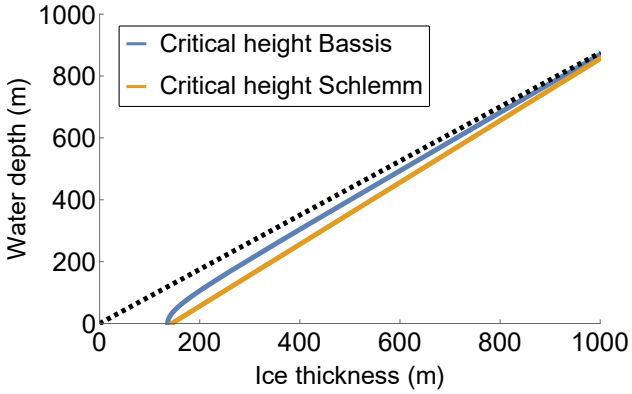

Figure 14: A comparrison between the critical height from Bassis et al. (2017) and Schlemm and Levermann (2018). The dashed line represents ice at flotation, while the blue and oranges line are critical height as function of water depth in the same fashion as figure 5.

The expression from Pollard et al. (2015) (equation (17)) however, does not correspond very well with the critical height from Bassis et al. (2017), while it claims to be derived from this very article. This cannot be shown easily analytically, but figure 15 shows how during a run of the model many grid points that do meet

the critical height as in equation (11), are not included in the grid points where calving takes place according to the expression from Pollard et al. (2015) (equation (17)) and vice versa. The reason for this, is that there is a substantial amount of crevassing needed to meet the condition set in equation (16). This results in cliffs that are not very much penetrated by crevasses having no calving at all, while they might exceed the critical height in equation (11). The other way round, some very crevassed cliffs may not meet the condition from Bassis et al. (2017), but do result in a lot of ice wastage when put in the expression from Pollard et al. (2015). There is simply a discontinuity between these two conditions.

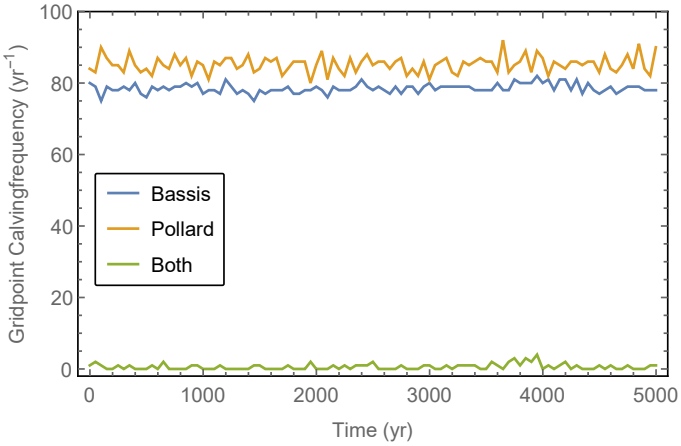

Figure 15: The number of grid points in the model for which calving occurs within a model time step. These results are from a simulation that is in steady state and which is obtained by running the model with current temperature. The blue and orange lines represent amount of grid points that have calving according to the expression by Bassis et al. (2017) and Pollard et al. (2015) respectively. The green line is overlap between the two, so grid points that have calving according to both expressions.

However, the expression for cliff calving wastage from Schlemm and Levermann (2018) (equation (19)) solely depends on ice height (H) and water depth (D). Logically however, you would expect an ice cliff to break off more easily when it has crevasses in it. The expression from Schlemm and Levermann (2018) does not account for this process, while the expression from Pollard et al. (2015) (equation (17)) does. On top of this, the expression from Schlemm and Levermann (2018) does not a account for hydrofracturing, which is the process that accounts for the massive increase in cliff failure calving according to DeConto and Pollard (2016).

In conclusion, the parametrisation of Pollard et al. (2015) has a lot of faults that the paremetrisation from Schlemm and Levermann (2018) does not have. However, the latter does not directly account for crevasses due to stress and hydrofracturing. It is therefore important to analyse results of experiments using both parametrisations and to draw conclusions accordingly taking the aspects of both parametrisations in mind. Nevertheless, a slight preference goes out to the expression by Schlemm and Levermann (2018) due to the arguments presented above.

5 Results

5.1 Climate response of cliff failure calving

To test the response and sensitivity of the ANICE model with just the cliff failure calving process added, the model is ran using a climate forcing that covers a spectrum of cold and warm temperatures. This forcing can be seen in figure 16. We start off using the initial ice sheet and a temperature of 8 K under present mean Antarctic temperature. We then increase the temperature every 30,000 years (30kyr) by 2 K using a sudden increase as can be seen in figure 16a. This is continued till 8 K above current temperature is reached for a total of 270kyr. Sea level forcing is done in a similar way to experiments done in de Boer et al. (2013). We start with 120 metres under modern global sea level and add 20 metres for every degree Kelvin that is added to the temperature until modern global sea level is reached as can be seen in figure 16b. Furthermore, insolation is taken to be at current levels.

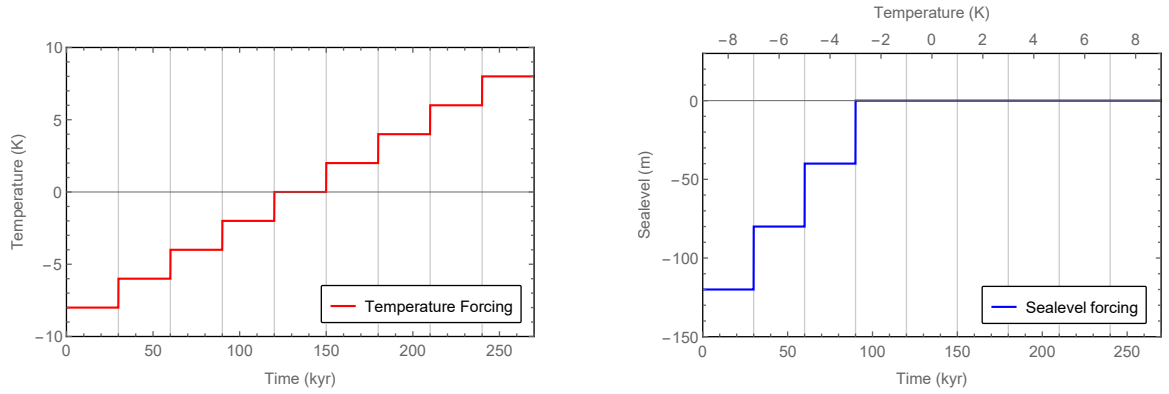

(a) **(b)**

Figure 16: Temperature and sea level forcing as a function of time. A sawtooth like function is used for the temperature (figure 16a) and a sea level forcing that corresponds to the temperature forcing is used (figure 16b).

These conditions are imposed on the model, using three different ways for cliff failure calving. Firstly, a reference simulation, where no calving takes place at all. Secondly, a simulation that uses the calving module as described in chapter 3.2.1 where equation (17) from Pollard et al. (2015) is used to calculate calving wastage. Thirdly, a simulation that uses the calving module as described in chapter 3.2.1 where equation (19) from Schlemm and Levermann (2018) is used to calculate calving wastage. No shelf calving is used in this experiment, except for removing unrealistically small shelves of 100 metres and under. This 100 metre boundary is also used for all other experiments in chapter 5. Subsequently, the resulting total shelf volume of Antarctica can be seen in figure 17b. Note that this ice shelf loss is not due to calving, but due to other processes. Also, the resulting sea levels, calculated using equation (30), can be seen in figure 17a.

The total shelf calving does not have a great dependency on what kind of cliff calving is used. As can be seen in figure 17b, only slight variations between simulations take place, with exception of a spike between 150 kyr and 160 kyr (when the temperature is increased from 0 K to 2 K) of the simulation that uses cliff calving as in Pollard et al. (2015) (equation (17)). The data of shelf volume is useful however to explain the difference in changes in sea level of the different simulations.

Figure 17a shows that steady states in sea levels and therefore in total ice volume are reached for all temperatures with the exception of extremely high and low temperatures (-8 K, 6 K and 8 K relative to modern temperature). As can be seen in figure 17a, during cold periods of 8 K under present temperature to 2 K under present temperature, there is almost no cliff calving whatsoever. When the temperature is subsequently forced to modern heights, there is a change between the reference simulation and the simulation that uses cliff calving from Pollard et al. (2015), which ends up in a steady state that is about 1 metre above the steady state that is obtained using no cliff calving. From then on, with increased temperature, both types of

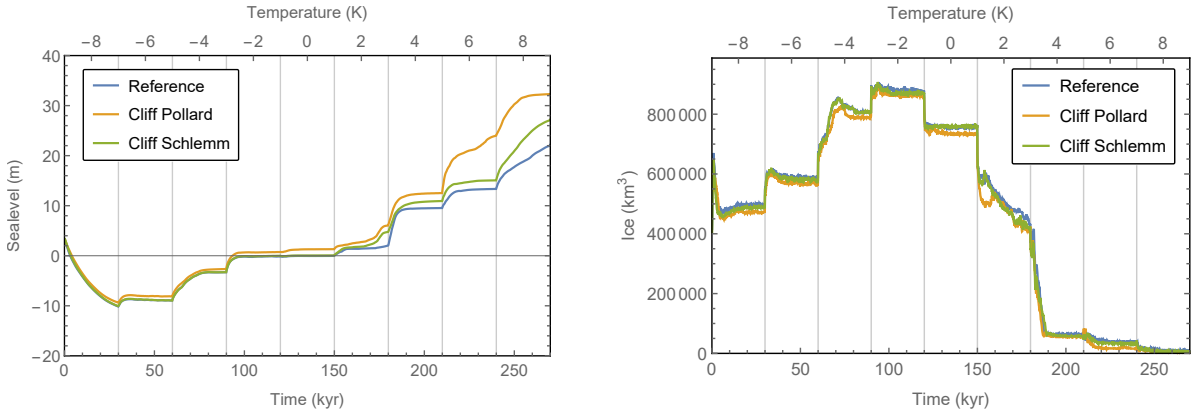

(a) **(b)**

Figure 17: Total Antarctic ice shelf volume and sea level increase as function of enforced temperature and sea level conditions. Shelf calving is not used in these simulations. Temperature and sea level are enforced as in figure 16. Figure 17a shows sea levels as function of time and temperature and figure 17b shows shelf volume as function of time and temperature. The *different colours* indicate: *blue* a reference simulation without cliff calving, *orange* a simulation with cliff calving using equation (17) (Pollard et al., 2015), *green* a simulation with cliff calving using equation (19) (Schlemm and Levermann, 2018).

cliff calving consistently rise sea levels quicker and reach a steady state that has a higher sea level than the reference simulation. Moreover, using cliff calving from Pollard et al. (2015) results in a significantly faster rise in sea level and a steady state that has a higher sea level than using cliff calving from Schlemm and Levermann (2018) for all temperatures that are warmer than present-day Antarctic temperature.

On top of the significant contribution to sea level rising of cliff calving, we see that total shelf volume decreases significantly when temperature is increased. This can be seen in figure 17b. Sea level rise is directly dependent on Antarctic ice volume, which decreases when more ice is lost by cliff calving. There are more places where cliff calving takes place when there are less ice shelves, since more cliffs reach the sea directly as discussed in chapter 2.1.

To find which areas on Antarctica are most vulnerable to ice cliff calving and to determine if there is causality between shelf removal and increase in cliff failure, snapshots of the height of the ice on Antarctica are taken. These can be seen in figure 18. Figures 18a and 18d are taken in cold climate conditions (8 K under modern) for respectively no cliff calving and cliff calving using Schlemm and Levermann (2018) (equation (19)). Firstly, there is no significant difference between the two, which corresponds with figure 17a. Secondly, both the Ross and Filchner-Ronne ice shelves have made place for grounded ice, which explains the lack of ice shelf volume that can be seen in figure 17a. Figures 18b and 18e are taken in warm climate conditions (2 K above modern) for respectively no cliff calving and cliff calving using Schlemm and Levermann (2018). The Filchner-Ronne ice shelf is still relatively intact in both simulations, which means that there should be relatively little cliff calving taking place there, since there will not be many cliffs exposed. The Ross ice cliff however, has completely vanished. As can be seen by comparing figures 18b and 18e, this has given way to cliff calving. Namely, in figure 18e, cliff calving has caused a significant ice loss from the side of the Ross shelf that borders the WAIS. When increasing temperatures even higher (8 K above modern), shelves are lost completely as can be seen in figures 18c and 18f which represent no cliff calving and cliff calving using Schlemm and Levermann (2018) respectively. Particularly in the bottom and top left (figures 18c and 18f) of the EAIS there is significantly more ice loss when cliff calving is used compared to when no cliff calving is used.

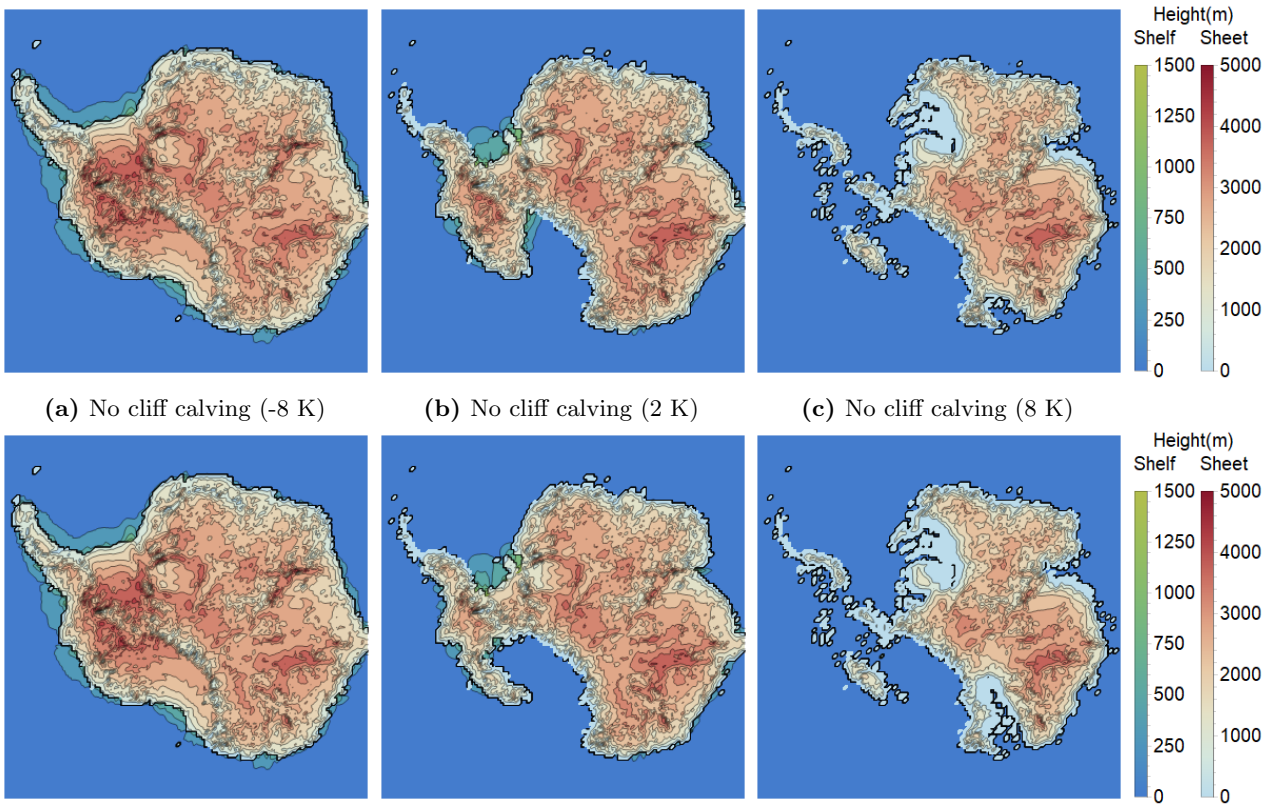

(a) No cliff calving (-8 K) **(b)** No cliff calving (2 K) **(c)** No cliff calving (8 K)

(d) Schlemm cliff calving (-8 K) **(e)** Schlemm cliff calving (2 K) **(f)** Schlemm cliff calving (8 K)

Figure 18: Topography of ice on Antarctica enforced by the temperature and sea level conditions as shown in figure 16. Ice height is shown for values between 0 and 5000 metres above sea level for ice sheets and values between 0 and 1500 metres above sea level for ice shelves as depicted on scales on the right side. 0 metres of ice sheet corresponds to land without ice. A black line divides shelf and sheet. The top row graphs are taken from the simulation where no calving was used. The bottom row graphs are taken from the simulation that uses cliff calving as in Schlemm and Levermann (2018) (equation (19)). Figures 18a and 18d show ice height after 30 kyr (8 K lower than modern temperature). Figures 18b and 18e show ice height after 180 kyr (2 K above modern temperature). Figures 18c and 18f show ice height after 270 kyr (8 K above modern temperature).

5.2 Calving during a glacial cycle

To test the accuracy of the model during realistic climate conditions a simulation of the previous glacial cycle is done. In order to simulate the glacial cycle temperature forcing based on benthic δ^{18}O data is used. The resulting temperature and sea level enforcing as function of time can be seen in figure 19a and are calculated as in de Boer et al. (2013). The resulting sea level change is shown in figure 19b. Like in the previous chapter, a reference simulation without any calving is done. Also, two simulations are done, both using no shelf calving, one using cliff calving from Pollard et al. (2015) (equation (17)) and one using cliff calving from Schlemm and Levermann (2018) (equation (19)). On top of this, the same two simulations, but also using shelf calving as in Pollard et al. (2015) (equation (26)) are done.

As can be seen in figure 19b, using just cliff calving has no significant effect on sea level changes, which is consistent with the notion that cliff failure calving has little effect during cold climate periods. However, when shelf calving is introduced a substantial rise in sea level compared to the reference simulation is observed as can be seen in figure 19b. A sea level rise is not what is expected when temperature decreases, which suggests that processes are overestimated in the parametrisation for shelf calving. This will be discussed further in chapter 6 and will be explored further in experiments in chapter 5.3.

The effect of introducing shelf calving can also be seen in figure 20, where Antarctica is shown during glacial maximum for simulations without shelf calving in figures 18b and 18d and for simulations with shelf calving in figure 18c and 18f. The difference is clear. Without shelf calving, regardless of whether cliff calving is used, the ice sheet covers all current day ice shelves. However when using shelf calving, ice shelves are removed and prevent growing ice back, which results in an ice sheet that can only shrink. This is not realistic as shelf calving wastage is overestimated. As said earlier, issues with shelf calving shall be further discussed in chapter 6. For now, we cannot interpret any simulations with shelf calving as realistic. However, it can serve as a tool to remove shelves in order to study ice cliff failure behaviour in other experiments.

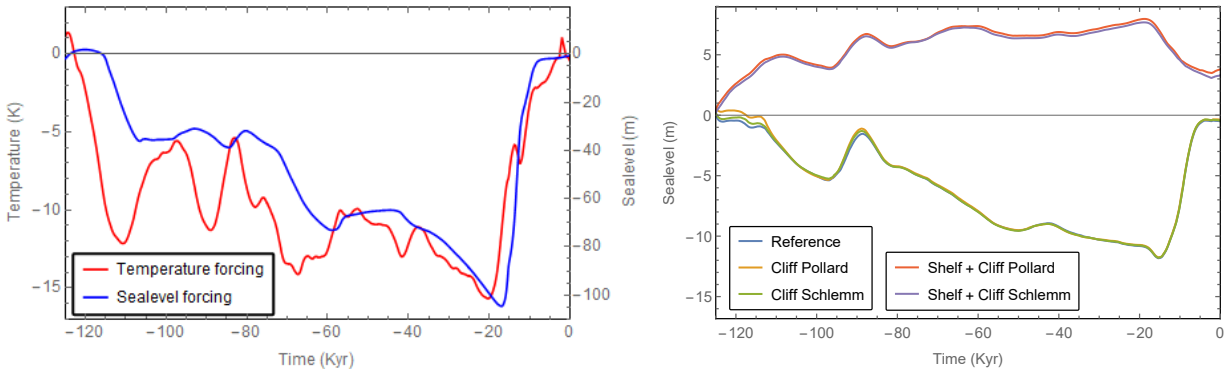

(a) **(b)**

Figure 19: Simulation of the last glacial cycle. The temperature and sea level forcing used is shown in figure 19a as function of time. The resulting sea level change is shown in figure 19b. The *different colours* indicate: *blue* a reference simulation with no calving, *orange* a simulation with no shelf calving and cliff calving as in Pollard et al. (2015) (equation (17)), *green* a simulation with no shelf calving and cliff calving as in Schlemm and Levermann (2018) (equation (19)), *red* a simulation using shelf calving and cliff calving as in Pollard et al. (2015), *purple* a simulation using shelf calving and cliff calving as in Schlemm and Levermann (2018).

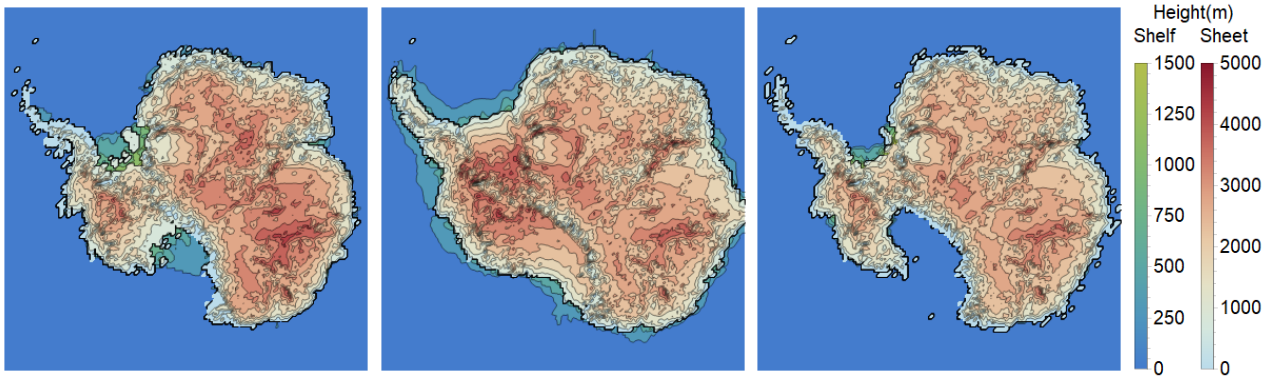

(a) Current **(b)** No shelf calving **(c)** Shelf calving

Figure 20: Topography of ice on Antarctica during the last glacial maximum. Ice height is shown for values between 0 and 5000 metres above sea level for ice sheets and values between 0 and 1500 metres above sea level for ice shelves as depicted on scales on the right side. A black line divides shelf and sheet. Figure 20a shows present-day conditions as reference. Figures 20b and 20c show Antarctica during the last glacial maximum, using no shelf calving (figure 20b) and using shelf calving (figure 20c).

5.3 Warm climate simulations

As is shown in the previous experiments, the initiation of cliff failure depends largely on the presence of ice shelves. In order to investigate this further, we compare sea level rises for different temperatures using cliff failure with or without shelf calving (equation (26)). As stated earlier, the shelf calving parametrisation should be seen as a tool to remove shelves in order to study cliff failure calving and not as accurately representing reality. The simulations done on glacial cycles show that cliff failure calving has no great effect in cold climates. We therefore stick to investigating climates that are warmer than or the same as the present climate. Figure 21 shows sea level rise for various combinations of shelf and cliff calving in current climate conditions. The simulation starts from a steady state that is reached using no calving at all and a forced temperature that corresponds with modern temperatures. Moreover, both the calving parametrisation from Pollard et al. (2015) (equation (17)) and the parametrisation from Schlemm and Levermann (2018) (equation (19)) are tested.

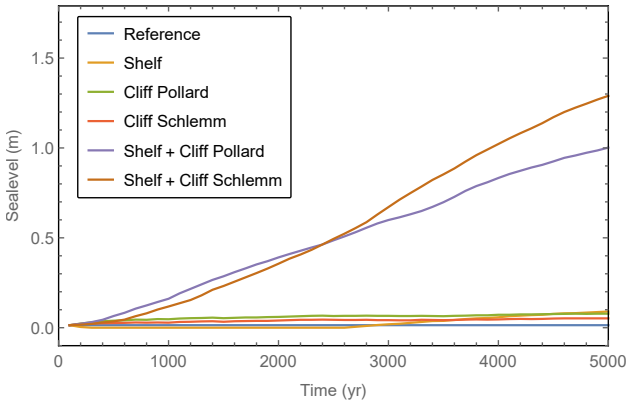

Figure 21: Sea level rises due to multiple combinations of calving processes at modern temperatures. The simulations start from a steady state that is reached in modern temperatures with no calving. The *different colours* indicate: *blue* a reference simulation with no calving, *orange* a simulation with just shelf calving, *green* a simulation with just cliff calving as in Pollard et al. (2015) (equation (17)), *red* a simulation with just cliff calving as in Schlemm and Levermann (2018) (equation (19)), *purple* a simulation using shelf calving and cliff calving as in Pollard et al. (2015), *brown* a simulation using shelf calving and cliff calving as in Schlemm and Levermann (2018).

As can be seen in figure 21, using just shelf calving or just cliff calving has none to nearly no influence on sea level rise. However, when both processes are used at the same time, additional sea level rises of at most 1.3 metres after 5000 years are reached. Both parametrisations predict this result, but disagree on the exact rate of sea level rise. Moreover, this result compares fairly well with results found by Pollard et al. (2015) that can be seen in figure 22, where global sea level rise as a result of simulations of Antarctica are shown for warm climate conditions. Note that Pollard et al. (2015) name one of the processes 'hydrofracturing' (figure 22), but this is actually referring to shelf calving. Also, the climate conditions between figure 21 and 22 are not comparable, as Pollard et al. (2015) use unspecified warm climate conditions. This explains the difference in magnitude of sea level rise. Furthermore, the initial rise and drop seen in sea level rises when using just one of the calving processes seen in figure 22 does not happen in the simulation in figure 21. However, Pollard et al. (2015) do not start from a steady state. Nevertheless, the notion that cliff failure calving is only a process of influence when another process that removes the shelves is introduced follows from both figures.

However, when the temperature is increased to 2 K above modern temperatures, just using cliff failure calving results in a greater increase in sea levels than using no calving at all as can be seen in figure 23. This is not consistent with the results in figure 22 from Pollard et al. (2015). Namely, just using cliff failure calving results in an additional increase in sea levels of 0.2 metres (100% relative to no calving, using Pollard et al. (2015)) or 0.6 metres (300% using Schlemm and Levermann (2018)). Nevertheless, using shelf calving as well as cliff calving still results in an even greater rise in sea levels. And the additional sea level rise when using both processes is greater than the sum of the additional sea level rise of using either process. This again,

indicates that as ice shelves are removed, the influence of cliff failure calving becomes greater.

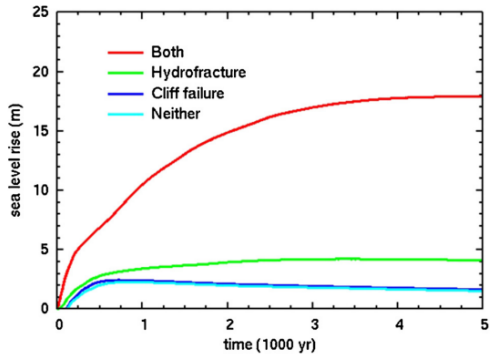

Figure 22: Global mean equivalent sea level rise in warm climate simulations from Pollard et al. (2015). The *different colours* indicate: *cyan* with neither cliff failure nor shelf calving, *blue* with cliff failure active, *green* with shelf calving, *red* with both these mechanisms active.

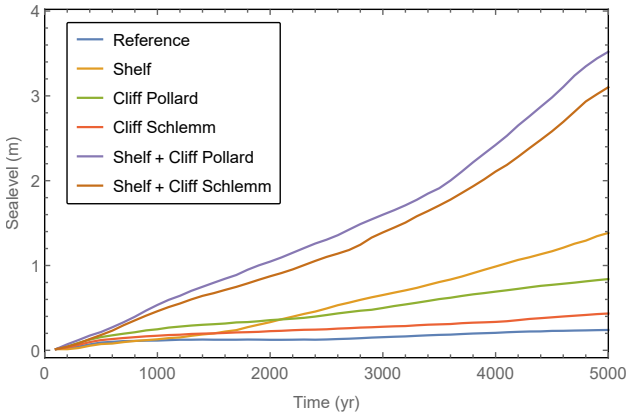

Figure 23: Sea level rises due to multiple combinations of calving processes at 2 K above modern temperatures. The simulations start from a steady state that is reached in modern temperatures with no calving. The *different colours* indicate: *blue* a reference simulation with no calving, *orange* a simulation with just shelf calving, *green* a simulation with just cliff calving as in Pollard et al. (2015) (equation (17)), *red* a simulation with just cliff calving as in Schlemm and Levermann (2018) (equation (19)), *purple* a simulation using shelf calving and cliff calving as in Pollard et al. (2015), *brown* a simulation using shelf calving and cliff calving as in Schlemm and Levermann (2018).

Moreover, figure 23 shows that when using shelf calving as well as cliff calving, using the parametrisation from Pollard et al. (2015) (equation (17)) results in a higher sea level rise than when using the parametrisation from Schlemm and Levermann (2018) (equation (19)). However, simulations of modern temperatures show that the parametrisation from Schlemm and Levermann (2018) result in a higher sea level rise for the first circa 2500 years of the simulation. This could indicate that parametrisation from Pollard et al. (2015) is more sensitive to shelf retreat. This difference could also follow from the sensitivity to higher temperatures of the parametrisation from Pollard et al. (2015) that stems from crevassing due to hydrofracturing (equation (14)). Namely, this depends on available liquid water, which is more abundant in warmer climates. However, there must be some difference in sensitivity that comes from ice shelf abundance between the simulations using the parametrisation from Pollard et al. (2015) and the parametrisation from Schlemm and Levermann (2018). Namely, in the experiment at modern temperature depicted in figure 21, temperature is kept constant, while total shelf volume decreases due to shelf calving. Therefore, the increase of relative rate of sea level rise at around 2500 years in figure 21 of the parametrisation from Pollard et al. (2015) can only explained by a relatively high sensitivity to ice shelf retreat.

Finally, we have also performed simulations for an increase of present-day temperatures of 5 Ks. The results from these simulations are shown in figure 24, which show that at these temperatures cliff calving from Schlemm and Levermann (2018) have a relatively small influence on rise in sea levels. Namely about 0.8 metres (10% relative to no calving) additional sea level increase without shelf calving and 0.9 metres (11%) with shelf calving. Using cliff calving from Pollard et al. (2015) results in an additional 2.7 metres (34%) without shelf calving and 5.2 metres (65%) with shelf calving. This again supports the notion that cliff calving using the parametrisation from Pollard et al. (2015) is more sensitive to shelf retreat as well as the notion that it generally results in a greater increase in sea level rise, or in other words, more cliff failure calving. However, the notion that the magnitude of cliff failure relies on a process that removes the ice shelves is less apparent than in simulations with lower temperatures, but is still present. Namely, the additional sea level rise when using both processes is still greater than the sum of the additional sea level rise of using either process.

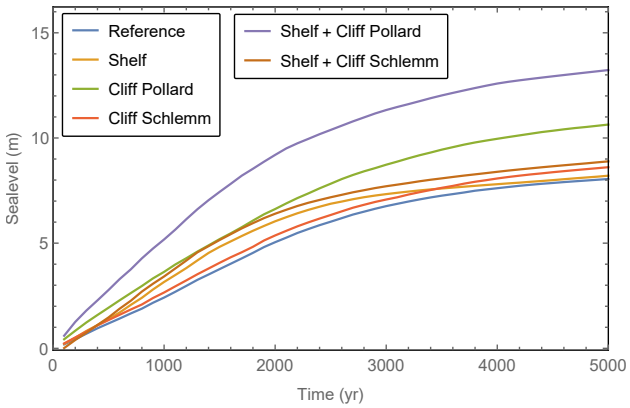

Figure 24: Sea level rises due to multiple combinations of calving processes at 5 K above modern temperatures. The simulations start from a steady state that is reached in modern temperatures with no calving. The *different colours* indicate: *blue* a reference simulation with no calving, *orange* a simulation with just shelf calving, *green* a simulation with just cliff calving as in Pollard et al. (2015) (equation (17)), *red* a simulation with just cliff calving as in Schlemm and Levermann (2018) (equation (19)), *purple* a simulation using shelf calving and cliff calving as in Pollard et al. (2015), *brown* a simulation using shelf calving and cliff calving as in Schlemm and Levermann (2018).

5.4 Ice recovery with cliff failure

To test the effect of cliff failure calving on recovery rates of ice shelves and sheets, simulations starting with severely retreated sheets as well as almost no ice shelves at all are done using modern temperatures. We simulate a period of 10 kyr using no shelf calving. When using no cliff calving, the ice sheet grows back at a rate of 9.8×10^5 km^3 in 10 kyr as can be seen in figure 25. The starting situation can be seen in figure 26a. The ice mostly grows back on the severely retreated WAIS as can be seen in figure 26b. Furthermore, some ice shelves are formed around this area, but not enough ice is gained to recover the complete WAIS or the major ice shelves in 10 kyr. As can be seen in figure 25, when applying cliff calving we get a smaller grow rate of 6.0×10^5 km^3 (62% relative to no calving) in 10 kyr when using cliff calving as in Schlemm and Levermann (2018) (equation (17)) and 1.4×10^5 km^3 (14%) in 10 kyr when using cliff calving as in Pollard et al. (2015) (equation (19)). This difference can be seen when comparing figures 26b and 26c that compare the Antarctic ice 10 kyr after the starting situation for no cliff calving (figure 26b) and cliff calving using Pollard et al. (2015) (figure 26c), which is the most extreme case. Cliff calving seems to result in a decrease in the ability for the ice sheet to recover after ice shelves and part of the sheets have been removed.

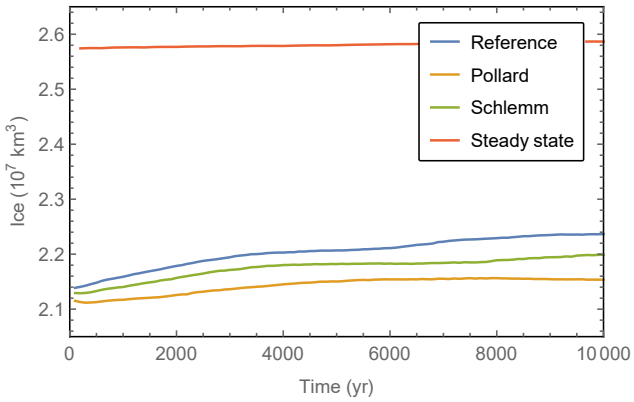

Figure 25: Ice sheet volume starting from extremely retreated ice shelves and sheets. The retreated sheet is as in figure 26a. Temperature is taken at modern temperature and shelf calving is not applied. The *different colours* indicate: *blue* a reference simulation with no calving, *orange* a simulation with cliff calving as in Pollard et al. (2015) (equation (17)), *green* a simulation with cliff calving as in Schlemm and Levermann (2018) (equation (19)), *red* the steady state that forms when current temperatures are applied and when we start with current Antarctic ice shelves and sheets (over a period of 100 kyr).

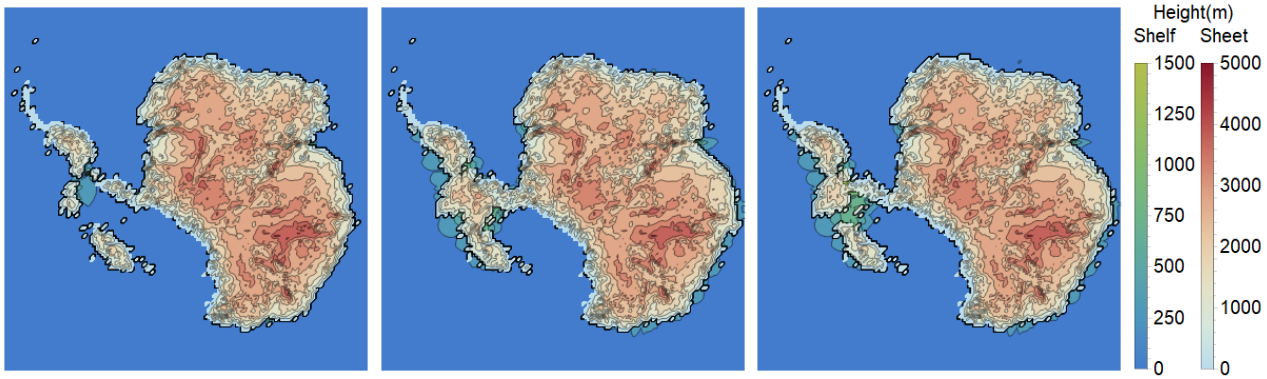

(a) Retreated sheet **(b)** No cliff calving **(c)** Pollard cliff calving

Figure 26: Topography of ice on Antarctica starting from extremely retreated ice shelves and sheets. Figure 26a shows starting conditions, having nearly no ice shelves left and most of the WAIS gone. Figures 26b and 26c show shelf and sheet regrowth after 10 kyr using no calving and using cliff calving from Pollard et al. (2015) (equation (17)) respectively.

5.5 The effect of hydrofraturing

To study the direct influence of crevassing by hydrofracturing (equation (14)) on cliff failure rates, we performed simulations in a relatively warm climate (2 K above modern temperature) are done. A relatively warm climate is chosen to ensure there is enough liquid water for hydrofracturing to have an effect. Only the parametrisation by Pollard et al. (2015) (equation (17)) is studied, since the parametrisation by Schlemm and Levermann (2018) (equation (19)) does not depend on the hydrofracturing process. Both shelf and cliff calving are used for these simulations. The sea level rises that result from these simulations can be seen in figure 27. Under these circumstances, hydrofracturing is responsible for an aditional sea level rise of 0.093 metres (2.7% relative to no hydrofracturing) over 5 kyr. Other warm climate simulations predict similar results.

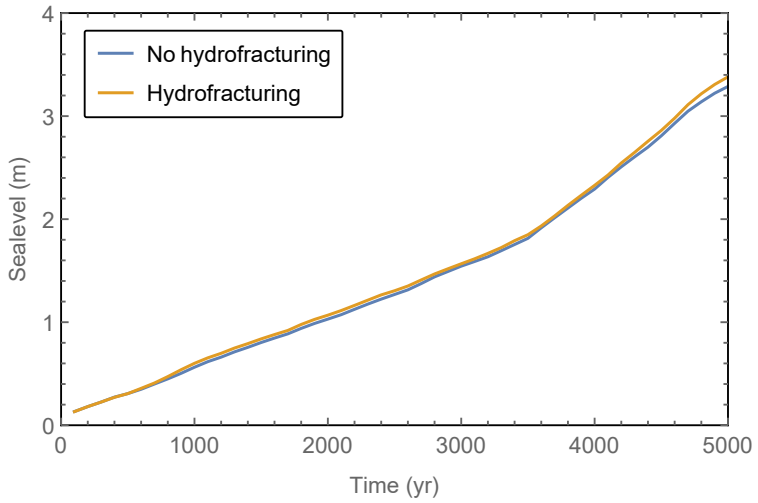

Figure 27: Sea level rise enforced by hydrofracturing. These simulations are done at 2 K above modern temperature and start from a steady state that forms from modern temperatures (the same conditions as in figure 23). Both shelf calving and cliff calving are applied as in Pollard et al. (2015) (equations (26) and (17)). The *different colours* indicate: *blue* a simulation without hydrofracturing applied, *orange* a reference simulation with hydrofracturing applied.

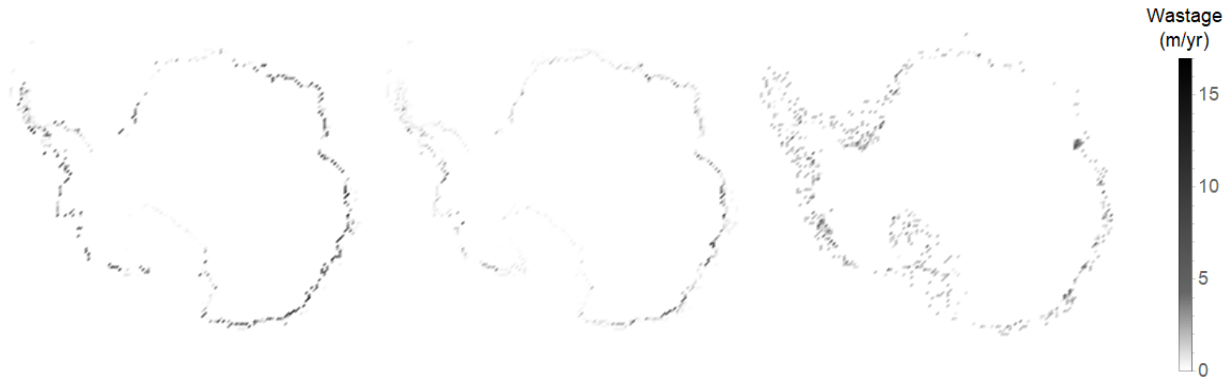

(a) Pollard cliff calving **(b)** Schlemm cliff calving **(c)** Shelf calving

Figure 28: Average vertical calving wastage during a glacial cycle (125 kyr, see chapter 5.2). The average is computed from 13 frames that are taken every 10 kyr starting at 0. Figure 28a shows average vertical wastage per grid point as a result of cliff calving when using cliff calving as in Pollard et al. (2015) (equation (17)). Figure 28b shows average vertical wastage per grid point as a result of cliff calving when using cliff calving as in Schlemm and Levermann (2018) (equation (19)). Figure 28c shows average vertical wastage per grid point as a result of shelf calving when using cliff calving as in Pollard et al. (2015), which is similar to the shelf calving when using cliff calving as in Schlemm and Levermann (2018).

5.6 Location of calving

To find spots that are particularly prone to cliff calving the vertical wastage per grid point per year is counted for the glacial cycle simulations (chapter 5.2) that use both shelf and cliff calving. This is done every 10 kyr starting at 0. The results are averaged over 125 kyr and can be seen in figure 28. Cliff calving seems to be largely equally distributed over grounding lines, with the exception of grounding lines that border ice sheets. However, as can be seen in figure 20c, during this simulation the Ross ice shelf is completely removed. This does not seem to result in much cliff calving in this area however. This result holds for both cliff calving parametrisations. The removal of the major ice shelves is supported by figure 28c, which shows the locations

of shelf calving during the glacial cycle using the same averaging method.

5.7 Magnitude of calving processes

A typical magnitude of cliff calving is 0 to 1000 Gton per year of ice wastage, depending on climate and shelf circumstances. To illustrate this, magnitudes of processes that add or remove ice from Antarctica are depicted in figure 29 from the warm climate simulation in chapter 5.3 that uses a temperature of 2 K above modern temperature. Shelf calving is also shown, but is still used as a tool rather than a realistic process. Figure 29 also shows the resulting magnitude of some other processes that take place on the bottom of ice shelves summarizes by bottom mass balance as a comparison. In this particular experiment, the average cliff calving magnitude when using Pollard et al. (2015) (equation (17)) is 250 Gton per year without shelf removal (figure 29a) processes and 360 Gton per year with shelf removal processes (29b). In the same way, the average cliff calving magnitude when using Schlemm and Levermann (2018) (equation (19)) is 120 Gton per year without shelf removal processes (figure 29c) and 190 Gton per year with shelf removal processes (figure 29d). These magnitudes are comparable to the bottom mass balance due to sub-shelf melting. A point of interest is that bottom mass balance is reduced when shelf calving is introduced. This is because the shelf calving process removes the shelves which means there is less ice prone to sub-shelf melting.

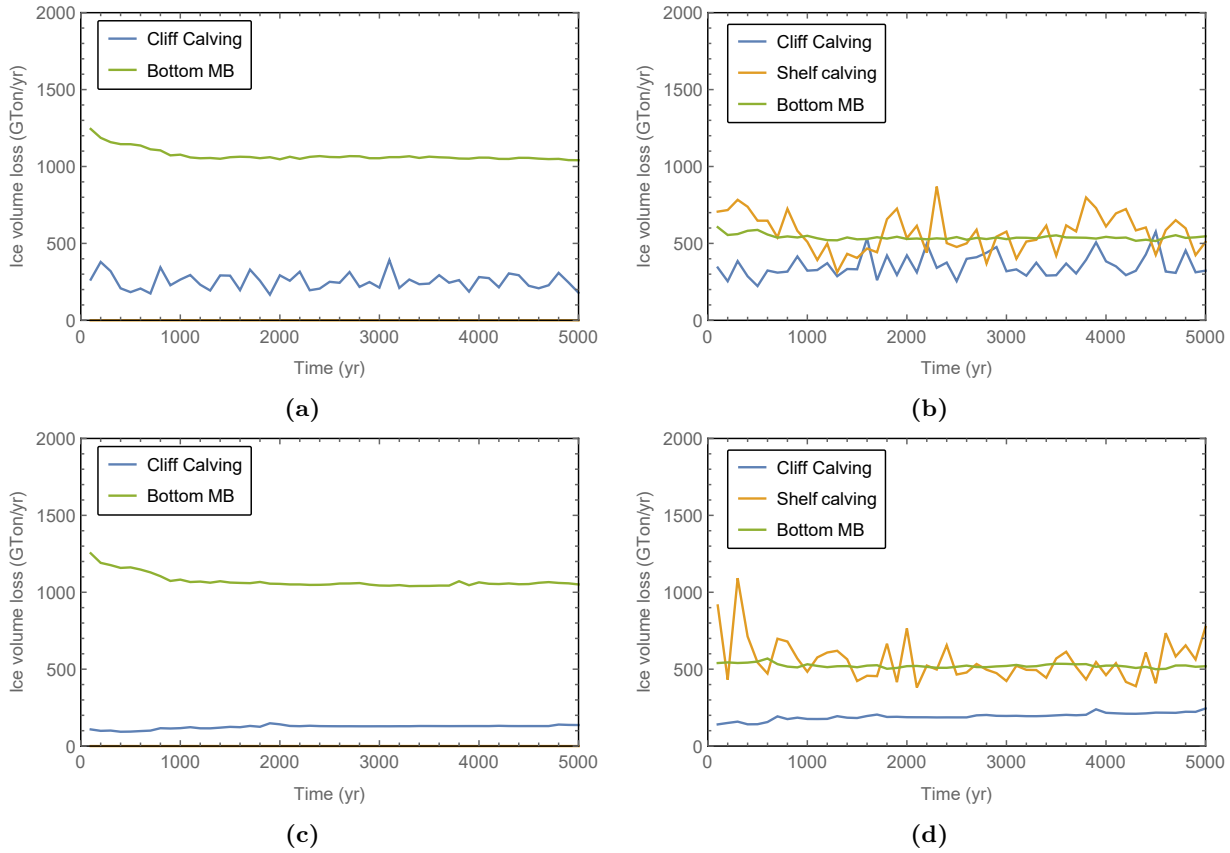

Figure 29: Magnitude of calving processes in a warm climate simulations (2 K above modern temperatures). Figure 29a uses just cliff failure calving from Pollard et al. (2015) (equation (17)). Figure 29b uses shelf removal and cliff failure calving from Pollard et al. (2015). Figure 29c uses just cliff failure calving from Schlemm and Levermann (2018) (equation (19)). Figure 29d uses shelf removal and cliff failure calving from Schlemm and Levermann (2018). The *different colours* indicate: *blue* ice volume (Gton) per year that is lost due to cliff calving, *orange* ice volume (Gton) per year that is removed from ice shelves by the process in equation (26), *green* ice volume (Gton) per year that is lost due to processes that affect the bottom of ice summarized as bottom mass balance.

5.8 RCP enforced future simulations

To predict future global sea level rise, we simulate the period of 2000 AD to 2500 AD enforcing climate conditions following from RCP predictions as described in chapter 2.4 and starting from a steady state that is reached at current temperatures. The temperature paths that are used are as in figure 11 (Pachauri et al., 2014). We do not use shelf calving as our parametrisation is not accurate. The results are shown in figure 30. The parametrisation from Pollard et al. (2015) (equation (17)) consistently predicts significantly higher sea level rises than the parametrisation from Schlemm and Levermann (2018) (equation (19)). Both give higher sea level rise predictions than using no cliff calving. In the worst case scenario (RCP 8.5 and using Pollard et al. (2015)) we see a predicted 2.9 metres global sea level rise. These results are not consistent with the 15 metres by 2500 AD that DeConto and Pollard (2016) predict. Nevertheless, from this experiment, it seems that cliff calving has a significant influence on future sea level rises.

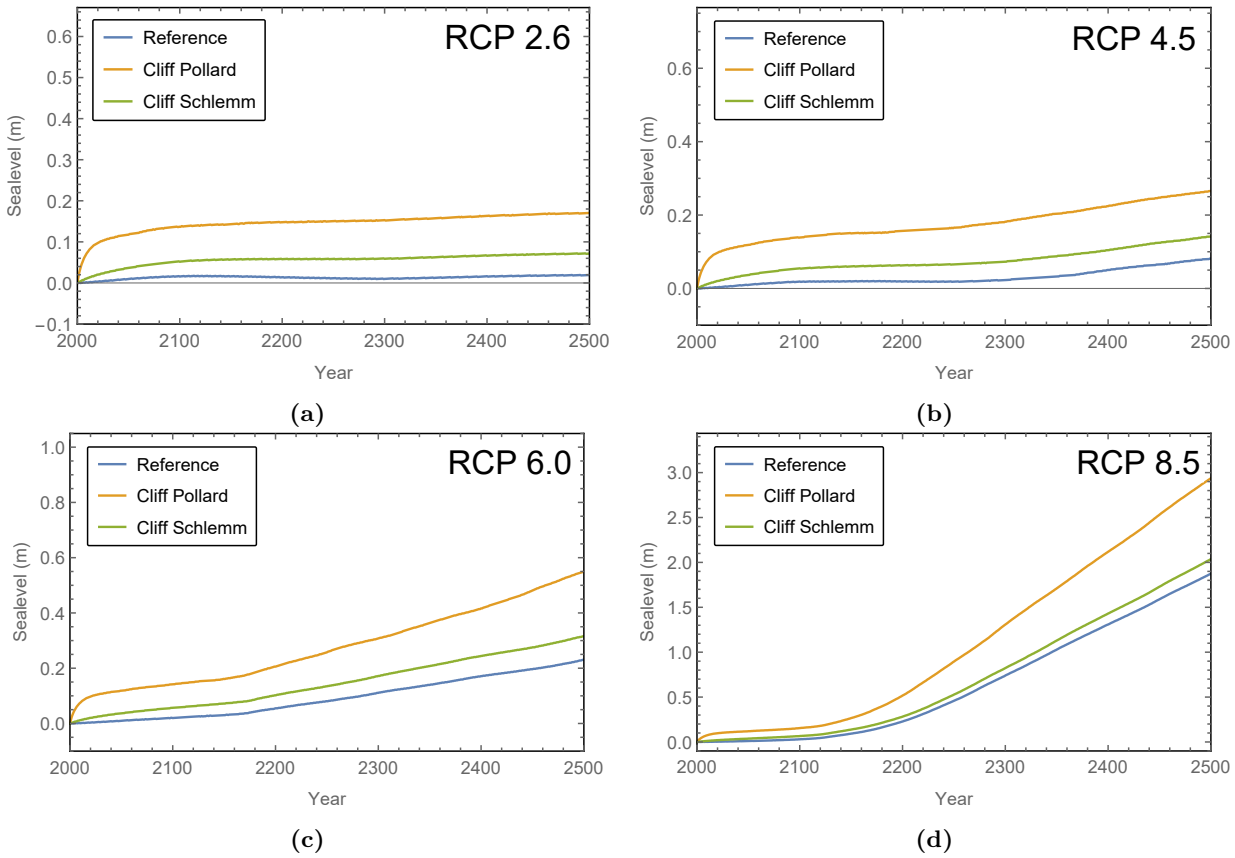

Figure 30: Sea level predictions for various RCP scenarios. No shelf calving is used and multiple ways of cliff calving are used. The *different colours* indicate: *blue* a reference simulation with no calving, *orange* a simulation with cliff calving as in Pollard et al. (2015) (equation (17)), *green* a simulation with cliff calving as in Schlemm and Levermann (2018) (equation (19)).

6 Discussions

An important issue is the fact that cliff failure wastage rates have a dependency on ice shelf conditions. Thus, in order to apply a cliff calving parametrisation one also needs a way to deal with shelf calving wastage. Historically, a way to implement such a process is to simply to use a critical value of ice thickness for which all floating ice is removed (e.g. de Boer et al. (2013)). It is questionable however, how accurately this depicts reality. What is certain however, is that the shelf calving parametrisation as used in this thesis (equation (26)) is not accurate as was seen in some of the experiments in chapter 5. One of the reasons for this is the use of the 100m boundary condition for the height of ice on top of the shelf calving from Pollard et al. (2015). This is implemented to prevent unrealistically small shelves forming near the grounding line and preventing cliff failure from happening. However, this accelerates shelf calving by removing complete grid points that are in the process of calving and would otherwise remain as ice shelves for a longer time. Yet, the main reason for this is that this parametrisation is meant for sub-grid use (Pollard et al., 2015). When applied to large grid points such as the one in the ANICE model, there is simply too much ice removed. A sub-grid interpolation with a fractional cover within the grid points should in general lower the amount of ice removed and should ensure a more accurate way of representing shelf calving. If this was to be used, shelf calving could be used as part of the calving process rather than a tool to remove shelves to study cliff calving like in this thesis.

Moreover, the general grid point size dependency of calving wastage magnitudes has a great uncertainty in results as consequence. Grid point size is not explicitly researched in this thesis, but is clearly an issue, since the calving parametrisation expressions that are used depend on grid size. Pollard et al. (2015) also acknowledge this problem. A solution for this problem would be sub-grid interpolation. An interpolation of the grounding- and calving line could be implemented using sub-grid point sizes of marginally smaller size than the grid point sizes (e.g. 1km$\times$1km). This would not increase computational cost greatly, as only grid points that lie on the border of the ice sheet or shelf would use interpolation. Ice calving wastage would still be applied vertically and the horizontal wastage term in equations (17) and (19) would be calculated per sub-grid point. Any horizontal wastage that would exceed the size of a sub-grid point could still be applied on the grid point, which would be comparable to having a horizontal wastage that goes beyond the sub-grid point to other sub-grid points within the ice sheet. Interpolation of the grounding line could be implemented using a similar approach as Feldmann et al. (2014) who use a linear interpolation approach or as in Gladstone et al. (2010), who use a combination of a linear and non linear interpolation.

Using sub-grid interpolation of the grounding line would also improve on the issue that ice height data of a grid point does not accurately represent ice height at the grounding line, as it is simply an average of ice height on the grid point area. Ice height plays a major role in both the cliff calving parametrisation from Pollard et al. (2015) (equation (17)) and the cliff calving parametrisation from Schlemm and Levermann (2018) (equation (19)). However, Pollard et al. (2015) assumes ice cliffs being at the grounding line, while Schlemm and Levermann (2018) does not. One would expect more accurate results, especially using the parametrisation from Pollard et al. (2015), when using sub-grid interpolation. A similar issue stems from applying cliff failure wastage vertically and not horizontally. This would also be largely solved by sub-grid interpolation. The vertical appliance results in ice grid points that are too wide and have a lower ice height than they should have. Namely, in reality cliffs collapse only on the side of the ice sheet. By applying sub-grid interpolation, a more accurate 3D picture of the ice sheet in the grounding line would be computed. This also bypasses having to store ice height data on sub-grid points in order to paint an accurate picture of the grounding line. An argument could be made that the liquid-like characteristics of the ice sheet could result in the ice sheet compensating for horizontal lost wastage by compressing in order to replace the ice lost at the edge of the sheet, but this process does not work on a time scale that is short enough to justify vertical appliance of cliff failure wastage.

Issues that stem from the arguably poorly constructed cliff calving parametrisations were discussed in chapter 4. Especially the parametrisation for cliff calving from Pollard et al. (2015) suffers from consistency and accuracy problems. Various experiments (chapters 5.1, 5.3, 5.7 and 5.8) show a discontinuity between the parametrisation from Pollard et al. (2015) and the parametrisation from Schlemm and Levermann (2018). Namely, the parametrisation from Pollard et al. (2015) consistently predicts more global sea level rise than the parametrisation from Schlemm and Levermann (2018). This implies that at least one of the parametrisation is

not accurate. Based on chapter 4, there is a significant preference towards the parametrisation from Schlemm and Levermann (2018).

Furthermore, there is a clear discontinuity between results in this thesis and Pollard et al. (2015). Shelf removal as tested in chapter 5.3 does not result in as much of an increase of cliff calving as was found in Pollard et al. (2015). This might be due to differences in model sensitivity or due to differences in parametrisation implementations. Also, RCP simulations in chapter 5.8 give global sea level predictions of 2.9 metres in the same conditions that resulted in 15 metres in Pollard et al. (2015). It is also much lower than the 7 metres that Church et al. (2013) predict. However, it must be noted that ANICE is has mostly been tested on long intervals (e.g. de Boer et al. (2013)) of time and might therefore not be as accurate when simulating periods of only 500 years. Moreover, no shelf calving is used in RCP enforced simulations, which is not realistic. Therefore, the results in chapter 5.8 should be considered with care, which could explain the discontinuity with Pollard et al. (2015).

Moreover, the dependency of sea level rise on total ice shelf volume that follows in chapter 5.1 seems to be implicated by the decrease of shelf volume and increase of sea levels with increased temperature. Nevertheless, the possibility arises that both processes are simply caused by increasing temperature. However, Pattyn (2017) concludes that ice mass loss is heavily sensitive to grounding line conditions and Fürst et al. (2016) concludes that 'retreat of current ice shelf fronts will yield important dynamic consequences', which implies a dependency of sea level rise on ice shelf conditions.

Future research should include a proper way to parametrise shelf calving as well as use of a sub-grid interpolation for the grounding- and calving line. More experiments involving locational calving could be done to research particular vulnerable spots on Antarctica that are more prone to calving processes. More research could be done on the effect of sea level forcing on calving processes. Namely, one would expect less calving when sea level rises, which would mean a negative feedback on additional global sea level rise due to calving. Also, more experiments could be done to determine how much of the ice wastage due to calving processes is compensated by other processes. For example, when ice shelves are lost due to calving, they can not also be lost due to bottom melt from ocean warming. Both processes are especially prominent at the edges of shelves and it would be interesting to see how much overlap there is. This might give a more accurate picture of the magnitude of wastage lost due to calving processes. Furthermore, more experiments that cover ice sheet and shelf return rates could be done. Experiments on this topic are done in chapter 5.4, but this only covers very severely retreated shelves and sheets. A marginally retreated shelf or sheet might not suffer from difficulty to retreat due to cliff calving. Moreover, more research could be done into how much uncertainty comes with the numbers and graphs that are shown in this thesis. Multiple simulations with slightly varying coefficients could be done for example in order to determine these uncertainties. Finally, more research could be done on why particular locations are vulnerable or resistant to cliff failure calving. For example, chapter 5.6 shows relatively little cliff failure calving at the ice Ross cliff during a glacial cycle where the Ross ice shelf is mostly removed by extreme shelf calving processes. A possible reason could be that this area is shallow.

Furthermore, a deeper understanding of the processes that take place on ice sheets and shelves especially in Antarctica could drastically improve the accuracy of results. On top of that, more data on the calving processes would improve current parametrisations. Namely, there is especially little data on Antarctic ice cliffs, which are quite different in size from ice cliffs on other locations. Nevertheless, parametrisations like in Schlemm and Levermann (2018), that approach the problem using a 2D stokes equation are a step in the right direction and prove that this subject is being worked on presently from multiple angles. With relatively many uncertainties, there is certainly room for much improvement in the future and the expectation is that within the next few years much progression shall be made.

7 Conclusions

Cold climate simulations show a negligible effect of cliff failure calving during periods of 2K or colder than modern temperatures (chapter 5.1). This is also seen in simulations of the last glacial cycle, which is mostly colder than modern day temperature, and suggest that using cliff failure calving has no conflict with sea level records during the last glacial cycle.

Warm climate simulations show a significant additional increase in global sea level due to cliff failure calving (chapter 5.1 and 5.3). For example, when going from 0K to 5K above modern temperature, after 5 kyr, 11% of sea level rise can be attributed to cliff failure calving or mechanisms activated by cliff failure calving when using the parametrisation from Schlemm and Levermann (2018). An even higher contribution of 34% relative to simulations using no cliff calving is found when using Pollard et al. (2015). Other warm climate simulations give similar results. This suggests that ice cliff failure calving can have a significant influence on ice loss on Antarctica and can therefore lead to increase of the global sea level.

The effects of cliff failure calving becomes more prominent when mechanisms that remove ice shelves are introduced (chapter 5.3). In the simulation that is done from a steady state an increase of 1 metre when using the parametrisation from Schlemm and Levermann (2018) is seen in 5 kyr on top of the steady state. Using Pollard et al. (2015) finds an increase of 1.3 metres. Other simulations support this result as they all show that the global sea level rise due to shelf and cliff calving is greater than the sum of both effects combined. This suggests that if or when we get to the point that ice shelves start breaking off en masse due to global warming, we can expect an increase in ice loss due to cliff failure and therefore an even faster rising global sea level.

Furthermore, ice sheets seem less capable in recovering their mass when cliff failure calving is introduced (chapter 5.4). At modern temperatures and a forcefully severely retreated ice sheet and none existent shelves, 62% of ice is able to recover when using cliff failure calving as in Schlemm and Levermann (2018) compared to using no cliff failure at all, which means that return rates are reduced by 28%. A mere 14% is recovered when using Pollard et al. (2015). This suggests an even longer recovery time for ice sheet return in a situation where Antarctic ice sheets have retreated and global temperatures go down again. Crevassing due to Hydrofracturing seems to have no direct significant influence on cliff calving rates (chapter 5.5), but might still result in greater shelf calving rates. Magnitudes of ice wastage due to cliff failure calving are comparable to other processes such as bottom melt due to ocean warming. However, as calving reduces ice mass, magnitudes of other processes decrease as calving magnitude increases. There is less ice cliff calving on a ice shelf free grounding line that forms when the Ross ice shelf is removed compared to other ice shelf free grounding lines (chapter 5.6).

RCP enforced simulations with cliff failure calving show a worst case scenario of 3 metres global sea level rise by 2500 AD, without any ice shelf removal processes (chapter 5.8, RCP 8.5). Of this 3 metres, 1.1 metres is due to cliff failure calving when using cliff calving as in Pollard et al. (2015). Cliff calving using Schlemm and Levermann (2018) gives a more moderate result and predicts a contribution of cliff calving of 0.16 metres at most (RCP 8.5).

An analytic comparison between cliff calving parametrisations from Pollard et al. (2015) and Schlemm and Levermann (2018) show a predilection towards the parametrisation from Schlemm and Levermann (2018). Results from simulations do not confirm nor deny this bias (chapter 4), but using parametrisation from Schlemm and Levermann (2018) for future research is recommended and results gained from Schlemm and Levermann (2018) should be favoured in this thesis.

In conclusion, this thesis shows that cliff failure calving will most likely have a significant influence on the degradation of ice on Antarctica and consequently the rise of global sea levels. Especially if or when ice shelves start to retreat, the process of cliff failure calving could have a very significant role and result in a large additional global sea level rise.

A Appendix

This appendix shows that the expression for horizontal ice wastage per year from Pollard et al. (2015) in equation (17) has the form of a ramp, in the sense that it is zero in many circumstances, then shoots up rapidly and reaches its maximal value relatively fast. That it acts as a ramp as a for different values of the glacier freeboard can be seen in 7 in chapter 2.3. In figure 31 can be seen how maximum crevassing due to stress ($(d_s + d_b)/H = 0.5$) and minimum crevassing due to stress ($(d_s + d_b)/H = 0.26$) still result in a relation that results in a wastage in the form of a ramp.

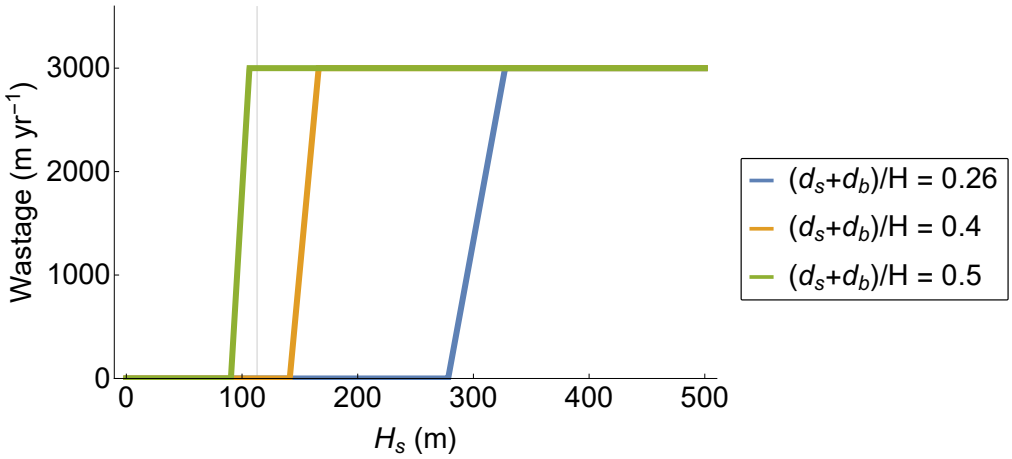

Figure 31: Horizontal wastage for cliff calving in m yr^{-1} as function of the glacier freeboard in m. The function is plotted for different values of the crevasse penetration ratio due to stress.

The same applies to changing the crevasse depth due to hydrofracturing (equation (14)). Figure 32 shows that having no hydrofracturing or very much hydrofracturing still results in a relation for the wastage in the form of a ramp.

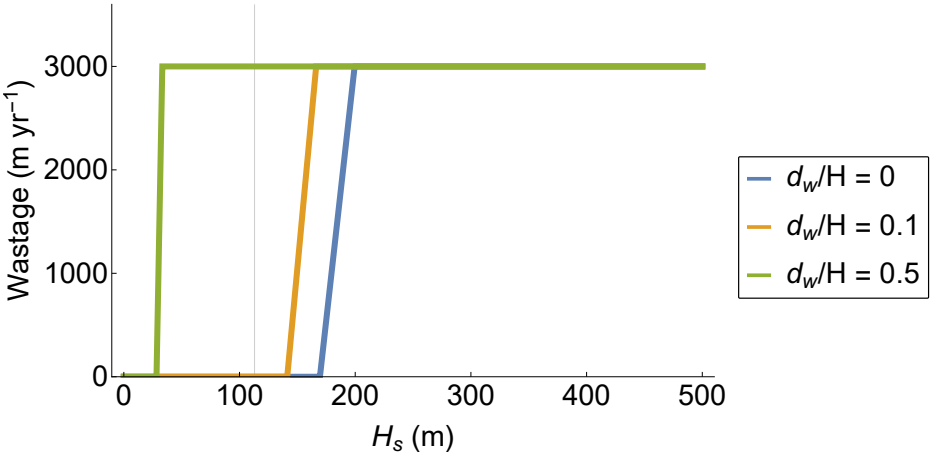

Figure 32: Horizontal wastage for cliff calving in m yr^{-1} as function of the glacier freeboard in m. The function is plotted for different values of the crevasse penetration ratio due to hydrofracturing.

Furthermore, the critical value from Pollard et al. (2015) of $h_c r \approx 113m$ is in principle given. However, changing it still does not change the ramp form of the expression in equation (17) as can be seen in figure 33. As a comparison, figure 8 in chapter 2 which shows the horizontal ice wastage from Schlemm and Levermann (2018) in equation (19) as a function of ice height and water depth shows that this expression does not express the ramp like behaviour.

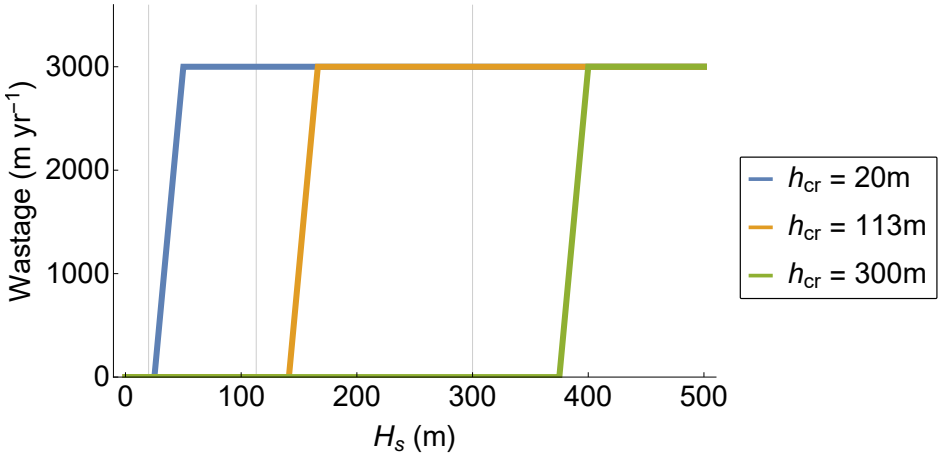

Figure 33: Horizontal wastage for cliff calving in m yr^{-1} as function of the glacier freeboard in m. The function is plotted for different values of the critical value h_{cr} as used by Pollard et al. (2015).

References

T. Albrecht, M. Martin, M. Haseloff, R. winkelmann, and A. Levermann. Parameterization for subgrid-scale motion of ice-shelf calving fronts. *The Cryosphere*, 5:35–44, 2011. doi: 10.5194/tc-5-35-2011.

J. N. Bassis and C. C. Walker. Upper and lower limits on the stability of calving glaciers from the yield strength envelope of ice. *The Royal Society*, 2011. doi: 10.1098/rspa.2011.0422.

J. N. Bassis, S. V. Petersen, and L. M. Cathles. Heinrich events triggered by ocean forcing and modulated by isostatic adjustment. *Nature*, 542:332–334, 2017. doi: 10.1038/nature21069.

J. A. Church, P. U. Clark, A. Cazenave, J. M. Gregory, S. Jevrejeva, A. Levermann, M. A. Merrifield, G. A. Milne, R. S. Nerem, P. D. Nunn, A. J. Payne, W. T. Pfeffer, D. Stammer, and A. S. Unnikrishnan. Sea level change. in: Climate change 2013: The physical science basis. contribution of working group i to the fifth assessment report of the intergovernmental panel on climate change. *Cambridge University Press*, 2013.

B. de Boer. *A reconstruction of temperature, ice volume and atmospheric CO2 over the past 40 million years*. PhD thesis, Utrecht University, 2 2012.

B. de Boer, R. S. W. van de Wal, L. J. Lourens, R. Bintanja, and T. J. Reerink. A continuous simulation of global ice volume over the past 1 million years with 3-D ice-sheet models. *Clim Dyn*, 41:1365–1384, 2013. doi: 10.1007/s00382-012-1562-2.

B. de Boer, A. M. Dolan, J. Bernales, E. Gasson, H. Goelzer, N. R. Golledge, J. Sutter, P. Huybrechts, G. Lohmann, I. Rogozhina, A. Abe-Ouchi, F. Saito, and R. S. W. van de Wal. Simulating the antarctic ice sheet in the late-pliocene warm period: Plismip-ant, an ice-sheet model intercomparison project. *The Cryosphere*, 9(3):881–903, 2015. doi: 10.5194/tc-9-881-2015.

R. M. DeConto and D. Pollard. Contribution of Antartica to past and future sea-level rise. *Nature*, 531: 591–597, 2016. doi: 10.1038/nature17145.

J. Feldmann, T. Albrecht, C. Khroulev, F. Pattyn, and A. Levermann. Resolution-dependent performance of grounding line motion in a shallow model compared with a full-stokes model according to the mismip3d intercomparison. *Journal of Glaciology*, 60:220, 2014. doi: 10.3189/2014JoG13J093.

J. J. Fürst, G. Durand, F. Gillet-Chaulet, L. Tavard, M. Rankl, M. Braun, and O. Gagliardini. The safety band of antarctic ice shelves. *Nature Climate Change*, 6:479–482, 2016. doi: 10.1038/nclimate2912.

R. M. Gladstone, A. J. Payne, and S. L. Cornford. Parameterising the grounding line in flow-line ice sheet models. *The Cryosphere*, 4:605–619, 2010. doi: 10.5194/tc-4-605-2010.

I. Joughin, B. E. Smith, and B. Medley. Marine ice sheet collapse potentially under way for the thwaites glacier basin, west antarctica. *Science*, 344:735–738, 2014. doi: 10.1126/science.1249055.

D. Macayeal. Largescale ice flow over a viscous basal sediment: Theory and application to ice stream b, antarctica. *Journal of geophysics*, 94:40714087, 1989. doi: 10.1029/JB094iB04p04071.

F. M. Nick, A. Vieli, M. L. Andersen, I. Joughin, A. Payne, T. L. Edwards, F. pattyn, and R. S. W. van de Wal. Sea level projections to ad2500 with a new generation of climate change scenarios. *Global and Planatary Change*, 80, 2012.

J. F. Nye. The distribution of stress and velocity in glaciers and ice-sheets. *The Royal Society*, 239:113–133, 1957. doi: 10.1098/rspa.1957.0026.

R. K. Pachauri, L. A. Meyer, and the core writing team. Climate change 2014: Synthesis report. Contribution of working groups i, ii and iii to the fifth assessment report of the intergovernmental panel on climate change. IPCC, 2014. Geneva, Switzerland, 151 pp.

F. Pattyn. Sea-level response to melting of antarctic ice shelves on multi-centennial timescales with the fast elementary thermomechanical ice sheet model (f.etish v1.0). *The Cryosphere*, 11:1851–1878, 2017. doi: 10.5194/tc-11-1851-2017.

D. Pollard and R. M. DeConto. Description of a hybrid ice sheet-shelf model, and application to antarctica. *Geoscientific Model Development*, 5:1273–1295, 2012. doi: 10.5194/gmd-5-1273-2012.

D. Pollard, R. M. DeConto, and R. B. Alley. Potential Antarctic ice sheet retreat driven by hydrofracturing and ice cliff failure. *Earth and Planetary Science Letters*, 412:112–121, 2015. doi: 10.1016/j.epsl.2014.12.035.

C. J. Ryan, A. L. Hubbard, E. Jasen, J. Todd, P. Christoffersen, J. R. Carr, O. Tom, and A. Neal. Uav photogrammetry and structure from motion to assess calving dynamics at store glacier, a large outlet draining the greenland ice sheet. *The Cryosphere*, 9:1–11, 2015. doi: 10.5194/tc-9-1-2015.

T. A. Scambos, E. Berthier, and C. A. Shuman. The triggering of subglacial lake drainage during rapid glacier drawdown: Crane glacier, antarctic peninsula. *Annals of Glaciology*, 52:74–82, 2011. doi: 10.3189/172756411799096204.

T. Schlemm and A. Levermann. Towards a parametrization of cliff calving. 2018.

J. Severinghaus and E. Brook. Abrupt climate change at the end of the last glacial period inferred from trapped air in polar ice. *Science*, 286:930–934, 1999. doi: 10.1126/science.286.5441.930.

C. J. van der Veen. Tidewater calving. *Journal of Glaciology*, 42:375–385, 1996.